MICROBIOLOGY

# Disruption of epithelium integrity by inflammation-associated fibroblasts through prostaglandin signaling

Yi Dong[1], Blake A. Johnson[1], Linhao Ruan[1], Maged Zeineldin[2], Tianhao Bi[2], Albert Z. Liu[1], Sumana Raychaudhuri[1], Ian Chiu[1], Jin Zhu[3], Barbara Smith[4], Nan Zhao[5], Peter Searson[5,6], Shigeki Watanabe[1], Mark Donowitz[7,8], Tatianna C. Larman[2]*, Rong Li[1,3,9]*



**Inflammation-associated fibroblasts (IAFs) are associated with progression and drug resistance of chronic inflammatory diseases such as inflammatory bowel disease (IBD), but their direct impact on epithelial cells is unknown. Here, we developed an in vitro model whereby human colon fibroblasts are induced by specific cytokines and recapitulate key features of IAFs in vivo. When cocultured with patient-derived colon organoids (colonoids), IAFs induced rapid colonoid expansion and barrier disruption due to swelling and rupture of individual epithelial cells. Colonoids cocultured with IAFs also show increased DNA damage, mitotic errors, and proliferation arrest. These IAF-induced epithelial defects are mediated by a paracrine pathway involving prostaglandin $E_2$ and its receptor EP4, leading to protein kinase A -dependent activation of the cystic fibrosis transmembrane conductance regulator. EP4-specific chemical inhibitors effectively prevented IAF-induced colonoid swelling and restored normal proliferation and genome stability. These findings reveal a mechanism by which IAFs could promote and perpetuate IBD and suggest a therapeutic avenue to mitigate inflammation-associated epithelial injury.**

## INTRODUCTION

Fibroblasts are a heterogeneous group of stromal cells that contribute to tissue architecture and support homeostasis of resident cells (*1*). Recent advances in single-cell multi-omics have provided insights into the diversity and functions of fibroblasts in normal and disease-affected tissues (*2*, *3*). Fibroblasts help maintain tissue integrity and homeostasis by secreting inflammatory mediators, producing growth factors and extracellular matrix (ECM) components, and facilitating the remodeling of tissue architecture after injury (*4*). However, under pathological conditions such as chronic inflammation, fibroblasts can be dysregulated to become inflammation-associated fibroblasts (IAFs) and contribute to pathogenic tissue fibrosis and scarring (*2*, *5*) and potentially other short- and long-term consequences.

Inflammatory bowel disease (IBD) is a chronic inflammatory condition affecting the intestine. Depending on the constellation of clinical symptoms and pattern of injury in the tubular gastrointestinal tract, IBD is partitioned into Crohn's disease (CD) and ulcerative colitis (UC). Its etiology is complex and multifactorial, but a key contributor to IBD pathogenesis is chronic epithelial barrier dysfunction that can instigate and propagate excessive immune responses (*6*). Chronic mucosal injury and repair can lead to mucosal remodeling including crypt architectural distortion, fibrosis, expanded lamina propria chronic inflammation, and epithelial metaplasia (*7*). IBD patients suffer from chronic diarrhea, fibrostenotic disease, and fissures, and carry increased risk of colitis-associated dysplasia and colorectal cancer (CAC) (*8*–*10*). CAC is characterized by early *TP53* mutations and widespread chromosome instability (CIN) (*11*, *12*). DNA damage and aneuploidy are observed even in nondysplastic IBD epithelium and likely plays a key role in CAC evolution (*13*). A recent human study reported that IBD colonic epithelium accrued twice the number of gene mutations and aneuploidy than normal colon epithelium (*10*). However, mechanisms by which the chronic inflammatory microenvironment in IBD promotes genome instability are poorly understood.

Because fibroblasts regulate the stemness, wound healing, and differentiation of intestinal epithelial cells (*14*), IAFs may play a role in IBD epithelial dysfunction. Recent scRNA-seq studies have defined *IL13RA2*$^+$*IL11*$^+$ fibroblasts as IAFs in IBD (*15*). These IAFs showed a strong association with immune signaling, ECM remodeling, and epithelial regulation (*16*). These IAFs were linked to resistance to biologics commonly used to treat IBD (*15*, *17*–*19*). Recent clinical studies have shown that reduction of IAFs is strongly associated with the responsiveness of IBD biologics, which mostly target immune cells (*17*, *20*, *21*). Moreover, animal studies have shown that IAFs correlate with poor prognosis of CAC (*22*, *23*). However, how IAFs interact with colon epithelium and affect its homeostasis remains elusive. Here, we develop an in vitro model of human colon–derived IAFs and use it to define cellular and molecular interactions between colon IAFs and epithelial cells. Our experimental findings uncover a paracrine pathway by which IAFs promote transepithelial fluid secretion, leading to impaired barrier function and cellular and genomic abnormalities in colon epithelium.

## RESULTS

### In vitro induction of IAFs from patient-derived fibroblasts

We first attempted to obtain IAFs from surgically resected colon tissues of IBD patients and from normal controls (Fig. 1A and

[1]Department of Cell Biology, Johns Hopkins School of Medicine, Baltimore, MD 21205, USA. [2]Department of Pathology, Division of GI/Liver Pathology, Johns Hopkins School of Medicine, Baltimore, MD 21205, USA. [3]Mechanobiology Institute and Department of Biological Sciences, National University of Singapore, Singapore, Singapore. [4]Microscope Facility, Johns Hopkins School of Medicine, Baltimore, MD 21205, USA. [5]Institute for Nanobiotechnology, Johns Hopkins University, Baltimore, MD 21218, USA. [6]Department of Materials Science and Engineering, Johns Hopkins University, Baltimore, MD 21218, USA. [7]Department of Medicine, Division of Gastroenterology, Johns Hopkins School of Medicine, Baltimore, MD 21205, USA. [8]Department of Physiology, Johns Hopkins School of Medicine, Baltimore, MD 21205, USA. [9]Department of Biological Sciences, National University of Singapore, Singapore, Singapore.
*Corresponding author. Email: tlarman1@jhmi.edu (T.C.L.); rong@jhu.edu (R.L.)

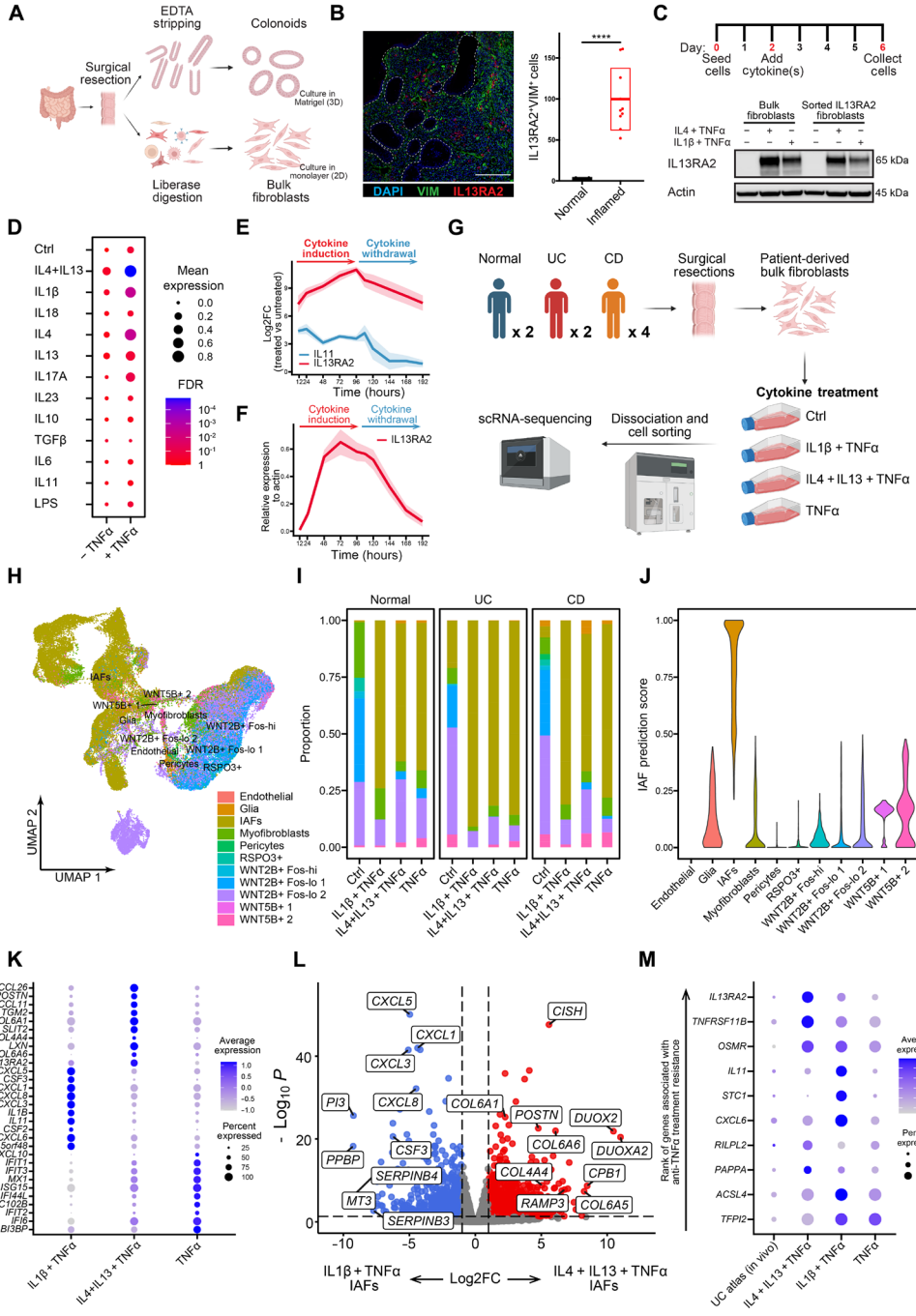


**Fig. 1. Generation of patient-derived fibroblasts and induction of IAFs.** (**A**) Schematic representation depicting the workflow for generating patient-derived bulk fibroblasts and colonoids. (**B**) Visualization of IAFs in human colonic mucosa. Left: Immunofluorescent image of a frozen human tissue section illustrating the presence of VIM$^{+}$IL13RA2$^{+}$ IAFs. White dashed lines represent the boundaries of epithelial cells; scale bar, 200 μm. Right: Number of IAFs in the field of view. Error box: SD. (**C**) In vitro expanded fibroblasts do not express IL13RA2 without cytokine stimulation. Top: Schematic representation depicting the workflow for activating fibroblasts using cytokine cocktails. Blot: Immunoblot showing expression of IL13RA2 in in vitro expanded fibroblasts treated with different cytokines. (**D**) Summary of IL13RA2 expression in fibroblasts treated with different cytokine cocktails. (**E**) mRNA expression of *IL13RA2* and *IL11* are inducible with the IL4 + IL13 + TNFα cocktail. Time course of qPCR assay showing mRNA expression of *IL13RA2* and *IL11* during cytokine induction and withdrawal. The line represents the mean and the shaded area represents SEM. (**F**) Protein expression of IL13RA2 is inducible with the IL4 + IL13 + TNFα cocktail. Time course of immunoblot assay showing IL13RA2 protein expression levels during cytokine induction and cytokine withdrawal. The line represents the mean and the shaded area represents SEM. (**G**) Schematic representation of the workflow for collecting, expanding, and treating patient-derived fibroblasts with different cytokine cocktails for scRNA-seq. (**H**) Cell census and cross reference of patient-derived fibroblasts. Shown is the UMAP of cells labeled by cell subsets. (**I**) IAFs are enriched after cytokine activation in in vitro expanded fibroblasts. (**J**) IAF census and similarity score. Violin plot showing the predicted IAF score of fibroblasts in each subset. (**K**) Subset-specific markers of different cytokine-treated fibroblasts. (**L**) DEGs that distinguish IL1β + TNFα versus IL4 + IL13 + TNFα IAFs. (**M**) Transcription profiles of genes previously shown to be associated with anti-TNFα treatment resistance in fibroblasts treated with different cytokines.

fig. S1A). We confirmed the presence of IL13RA2$^+$ VIM$^+$ IAFs, which were enriched in surgical resections from IBD patients (*15*) (Fig. 1B and fig. S1B). We then used a passive selection approach to enrich bulk fibroblasts (see details in Materials and Methods) from normal, UC, and CD samples (table S1). However, IL13RA2 immunoblotting of protein lysates from IBD-derived early passage bulk fibroblasts was negative, suggesting that IAFs were no longer present (Fig. 1C and fig. S1, C to F). To further investigate this, we cultured IL13RA2$^+$ fibroblasts directly sorted from fresh IBD patient tissue, but once again IL13RA2 expression was lost after a short expansion (four passages) in vitro (Fig. 1C). We hypothesized that IL13RA2$^+$ fibroblasts require a continuous pro-inflammatory environment to maintain their identity. We therefore treated bulk fibroblasts with interlukin-1β (IL1β), IL4, and tumor necrosis factor–α (TNFα), common cytokines detected in IBD colon mucosa (*24*–*26*). Cultured fibroblasts regained IL13RA2 expression after cytokine treatment (Fig. 1C and fig. S1, C to F), similar to a previous report in nasal polyp fibroblasts (*27*). This suggests that IL13RA2$^+$ fibroblasts may require continuous cytokine stimulation to maintain IAF characteristics.

To test the above hypothesis, we screened a panel of IBD-associated cytokines and inflammatory factors to determine which led to robust up-regulation of IL13RA2 in four UC, four CD, and three normal fibroblast (NF) lines (*24*–*26*). Most cytokines were insufficient to induce IL13RA2 up-regulation individually, although IL1β, IL4, IL13, and TNFα led to moderate up-regulation (Fig. 1D and fig. S1G). When combining T helper 1 ($T_H1$) cytokines IL1β and TNFα, two classic cytokines that activate fibroblasts in cancer (*28*), IL13RA2 expression was markedly up-regulated (Fig. 1D). However, $T_H2$ cytokines IL4 and IL13, in combination with TNFα, induced the strongest IL13RA2 expression (Fig. 1D). To determine the kinetics of IL13RA2 induction and turnover, we used the IL4 + IL13 + TNFα cytokine cocktail and performed a time-course experiment with 4 days of cytokine treatment followed by 4 days of cytokine withdrawal. Both the mRNA and protein level of IL13RA2 increased with cytokine treatment and decreased upon cytokine withdrawal (Fig. 1, E and F, and fig. S1F). These data show that IL13RA2+ fibroblasts can be induced from both normal and IBD colon-derived bulk fibroblasts, but their maintenance requires continuous presence of the cytokines.

To further evaluate the similarity between cytokine-activated fibroblasts as described above and IAFs in vivo, we performed single-cell RNA sequencing (scRNA-seq) of patient-derived bulk fibroblasts obtained from two UC samples, four CD samples, and two healthy controls (Fig. 1G and fig. S1H). The fibroblasts were treated for 4 days with either TNFα alone, IL4 + IL13 + TNFα, or IL1β + TNFα. Including control fibroblasts, 60,845 cells were recovered with mean reads of 75,614. Using a published reference mapping method (*29*), we compared single-cell gene expression profiles with a published UC atlas database (*15*) and confirmed that our cytokine-activated fibroblasts were enriched to the IAF category (Fig. 1H and fig. S1, I and J), compared to other populations (Fig. 1J and fig. S1K). Also consistent with the lack of IL13RA2 protein expression in early-passage non–cytokine-treated bulk fibroblasts (Fig. 1C), cells mapping to IAF were strongly enriched after cytokine induction (Fig. 1I). Fibroblasts treated with different cytokine cocktails showed unique gene expression signatures (Fig. 1K and fig. S1L). Comparing differentially expressed genes (DEGs) in IL1β + TNFα–activated fibroblasts revealed enrichment of genes involved in chemotaxis (e.g., *CXCL1*, *CXCL3*, *CXCL6*, *CXCL8*, *CXCL10*, *CSF2*, and *CSF3*) (Fig. 1, K and L). By contrast, IL4 + IL13 + TNFα–activated fibroblasts showed up-regulation of ECM genes (e.g., *COL4A4*, *COL6A1*, *COL6A6*, and *POSTN*), whereas fibroblasts treated with TNFα alone showed enrichment for genes downstream of interferon signaling (e.g., *IFIT1*, *IFIT2*, *IFIT3*, and *IFIT6*) (Fig. 1K). Although gene set enrichment analysis (GSEA) suggested that fibroblasts treated with either IL1β + TNFα or IL4 + IL13 + TNFα showed enrichment in pathways associated with immune responses (fig. S1, M and N), IL4 + IL13 + TNFα–activated fibroblasts showed significant enrichment in genes associated with collagen processing and ECM remodeling (Fig. 1L). These signatures are also significantly enriched in GSEA analysis of IAFs from IBD patients (fig. S1O). Additionally, IL4 + IL13 + TNFα–induced IAFs showed significantly higher expression of many previously reported IBD-associated IAF transcriptional signatures (*15*, *17*, *30*–*33*) compared to IL1β + TNFα–treated IAFs (fig. S1P). Last, the gene expression signature of IL4 + IL13 + TNFα–induced fibroblasts showed robust up-regulation of fibroblast genes previously ranked highly to be associated with IBD treatment resistance (*15*, *34*–*36*), such as *IL13RA2* and *TNFRSF11B* (Fig. 1M). Considering that $T_H2$ responses are up-regulated in chronic IBD (*25*), we conclude that IL4 + IL13 + TNFα–activated fibroblasts largely recapitulate IBD-associated IAFs in vivo. However, to differentiate them from IAFs in vivo, we refer to these IL4 + IL13 + TNFα–induced fibroblasts as induced IAFs (iIAFs) hereafter.

### IAFs induce colonoid swelling via paracrine signaling

Fibroblasts are known to regulate the morphology, expansion, and differentiation of epithelial cells in the intestinal crypt (*18*). To investigate how iIAFs affect colon epithelial organization and growth (fig. S2A), we established a coculture model combining either iIAFs or NFs with human colonoids (Figs. 1A and 2A; see Materials and Methods for details). To generate human colonoids, the EDTA-based stripping method was used to enrich crypts. Dissociated crypts were seeded in Matrigel and cultured for 4 days to form colonoids. In the meantime, iIAFs were induced using IL4 + IL13 + TNFα for 4 days. NFs or iIAFs were then cocultured with colonoids outside of the Matrigel. iIAF induction was followed by cytokine washout before coculturing with normal colonoids to avoid any direct effect of the cytokines on colonoids, but the duration of the coculture was only 24 hours before iIAFs lost their characteristics as shown in Fig. 1F. By using live-cell imaging, we observed that the luminal volume of colonoids increased dramatically when cocultured with iIAFs but not with NFs, accompanied by a reduction of apical-basal epithelial thickness (Fig. 2, B and C, fig. S2D, and movie S1). The same phenomenon was observed when transwells were used as a physical barrier between iIAFs and colonoids (fig. S2, B and C), suggesting that colonoid swelling did not require direct contact between iIAFs and epithelial cells.

To directly test whether iIAF-secreted paracrine factors caused colonoid swelling, we added colonoid culture media to fibroblasts and collected conditioned media (CM) from six different fibroblast lines (two UC, two CD, and two normal), with or without cytokine induction (Fig. 2D; see Materials and Methods for details). We first ruled out the possibility that colonoid swelling was induced by traceable amounts of iIAF-inducing cytokines (IL1β, IL4, IL13, or TNFα) after cytokine washout by treating colonoids with these cytokines directly (fig. S2E). CM were then used to culture colonoids (Fig. 2, E and F). In all colon fibroblast lines tested, CM produced by iIAFs

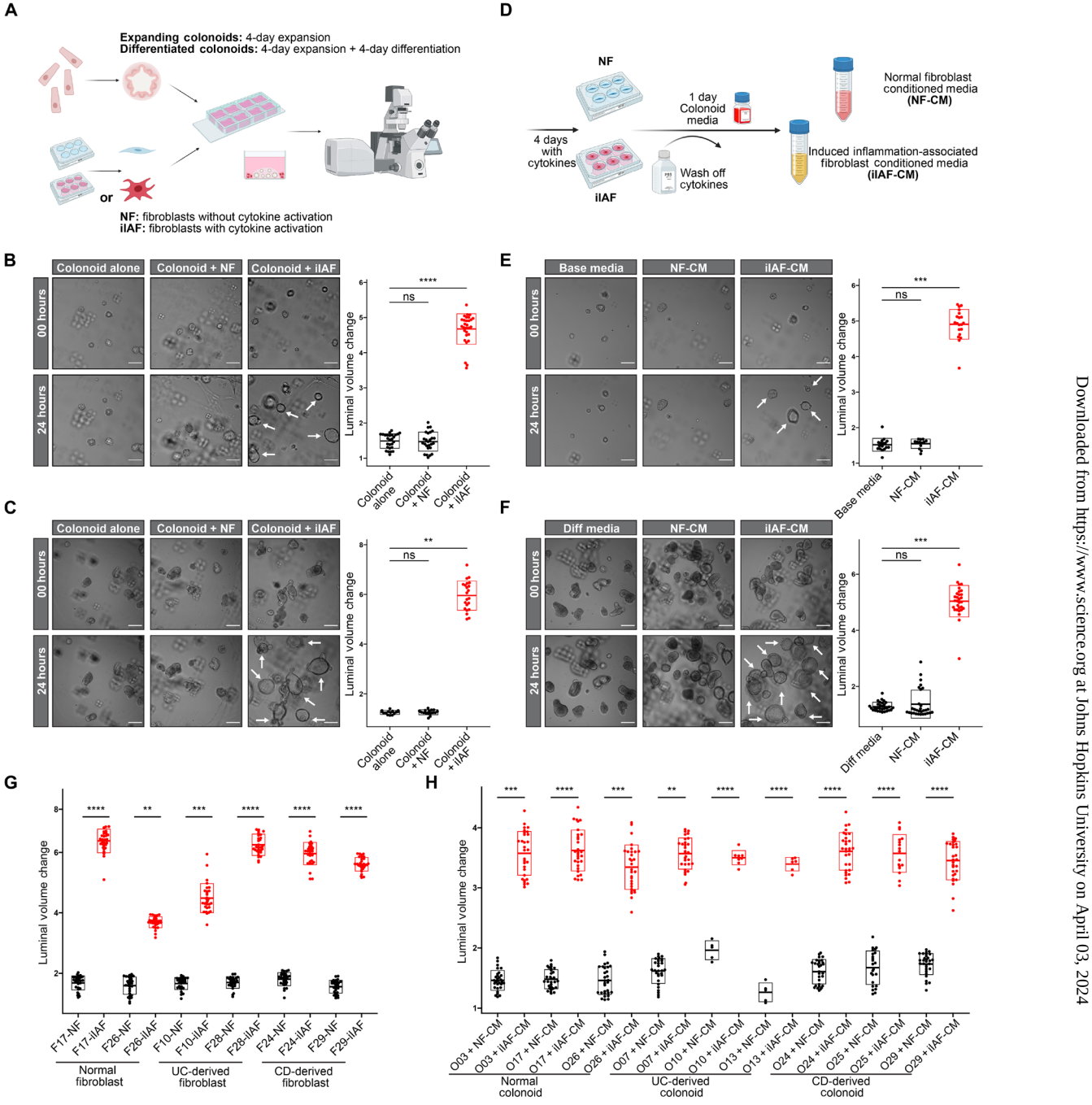


**Fig. 2. iIAFs induce colonoid swelling through paracrine signaling.** (**A**) Schematic representation of the workflow for colonoid-fibroblast coculture experiments. (**B**) iIAFs induce colonoid swelling in expanding colonoids. Left: Representative images of expanding colonoids cocultured with NFs or iIAFs. Arrows point to swelling colonoids cocultured with IAFs. Scale bars, 100 μm. Right: Box plots showing the degree of luminal volume change in expanding colonoids cocultured with NFs or iIAFs. Bar box represents mean ± SD, which also applies to (C) and (E) to (H). (**C**) iIAFs induce colonoid swelling in differentiated colonoids. Left: Representative images of differentiated colonoids cocultured with NFs or iIAFs. Arrows point to swelling colonoids cocultured with iIAFs. Scale bars, 200 μm. Right: Box plots showing the degree of luminal volume change in differentiated colonoids cocultured with NFs or IAFs. (**D**) Schematic representation of the workflow for generating fibroblast conditioned media (CM) for colonoid-fibroblast coculture experiments. (**E**) iIAF-CM induces colonoid swelling in expanding colonoids. Left: Representative images of expanding colonoids cultured in NF-CM or iIAF-CM. Arrows point to swelling colonoids under iIAF-CM. Scale bars, 100 μm. Right: Box plots showing the level of luminal volume changes of expanding colonoids cultured using NF-CM or iIAF-CM. (**F**) iIAF-CM induces colonoid swelling in differentiated colonoids. Left: Representative images of differentiated colonoids cultured in NF-CM or iIAF-CM fibroblast CM. Arrows point to swelling colonoids under iIAF-CM. Scale bars, 200 μm. Right: Box plots showing the level of luminal volume changes of differentiated colonoids cultured using NF-CM or iIAF-CM. (**G**) iIAFs from multiple fibroblast lines induce colonoid swelling. Box plots showing the degree of luminal volume change in colonoid O03 treated with NF- or iIAF-CM induced by six different fibroblast lines. (**H**) Multiple colonoid lines respond to iIAF-CM–induced swelling. Box plots showing the degree of luminal volume change in colonoid lines treated with NF-CM or iIAF-CM derived from fibroblast F26.

(iIAF-CM), but not NFs (NF-CM), induced colonoid swelling (Fig. 2G). Similar results were obtained when using iIAF-CM from one of the fibroblast lines to culture colonoid lines derived from normal, UC, and CD patients (Fig. 2H). These results confirmed that iIAFs induced colonoid swelling via paracrine signaling and that cytokine activation, rather than the source of fibroblasts or colonoids, was critical to induce colonoid swelling. This aligns with immunofluorescent staining of IBD colonic mucosa, which shows that iIAFs were scattered in the lamina propria and not directly interacting with colon crypts (fig. S2A). Because the various fibroblast and colonoid lines behaved similarly in coculture experiments, we used a representative normal colonoid line (O03) and a representative NF line (F26) in subsequent experiments.

### iIAF-induced colonoid swelling is associated with barrier leakage and cell rupture

To understand how iIAFs induce colonoid swelling, we first considered the possibility of increased epithelial cell proliferation. However, terminally differentiated colonoids similarly swelled in the presence of iIAF-CM (Fig. 2F and movie S2), arguing against this possibility (*37*). Next, we generated colonoids expressing H2B-mNeonGreen and tracked cell proliferation for 24 hours by live imaging. We observed fewer cell divisions in colonoids cultured in iIAF-CM compared to those in NF-CM (Fig. 3A and fig. S3A). The 5-ethynyl-2'-deoxyuridine (EdU) incorporation assay further confirmed reduced proliferation in iIAF-CM–cultured colonoids compared to those cultured in NF-CM (Fig. 3B and fig. S3B). These results suggest that the iIAF-induced colonoid swelling was not due to increased cell proliferation but was instead associated with impaired epithelial growth.

Time-lapse imaging showed that colonoids began to increase in luminal volume within minutes of iIAF-CM treatment, followed by a sudden volume reduction a few hours later (Fig. 3C and movie S3). Whereas the volume increase could be due to transepithelial fluid secretion, the collapse could be related to rupture of the epithelial barrier (Fig. 3C). To test this, we assayed epithelial permeability by adding 4 kDa fluorescein isothiocyanate (FITC)–dextran into the media (Fig. 3D). In NF-CM, there was no significant leakage of FITC-dextran into the colonoid lumen (*38*). In contrast, both nondifferentiated and terminally differentiated colonoids were susceptible to FITC-dextran leakage into the lumen when treated with iIAF-CM (Fig. 3, E and F, and fig. S3, C and D). These observations suggest that iIAF paracrine signaling can disrupt the barrier function of colon epithelium.

The barrier function of epithelia requires apical-basal polarity and polarized formation of tight junctions (*39*). Immunofluorescent (IF) staining of both tight junctions (stained using anti-ZO-1) and cell polarity markers (actin, stained with phalloidin) revealed that epithelial cells in colonoids cultured in iIAF-CM lost their normal columnar morphology and became stretched circumferentially (Fig. 3G and fig. S3E). However, thin-sectioning electron microscopy showed that epithelial junctions appeared largely intact in IAF-CM–treated colonoids (Fig. 3H and fig. S3F). Similar results were observed in colonoids expressing mNeonGreen::ZO-1 (fig. S3, G to J). These data suggest that tight junctions remain largely present in colonoids treated with iIAF-CM but do not shed light on their functional integrity.

To observe dynamic epithelial changes during iIAF-induced colonoid swelling, we performed live-cell imaging using colonoids expressing plasma membrane–anchored red fluorescent protein (mCherry-CAAX) and labeled with SiR-Actin, a live-actin probe (*40*). In conjunction with the FITC-dextran permeability assay, we observed that individual epithelial cells were larger in colonoids cultured in iIAF-CM than those in NF-CM (Fig. 3I), and FITC-dextran leakage into the cell was associated with marked swelling and rupture of individual cells in colonoids (Fig. 3, C and J), which was associated with a rapid increase of FITC-dextran signal in the colonoid lumen (Fig. 3K). These observations suggest that cell rupture is a cause of epithelial barrier disruption during swelling.

### iIAF-induced colonoid swelling is PKA and CFTR dependent

The rapid increase of colonoid luminal volume suggests transepithelial fluid secretion into the lumen, a process contributing to diarrhea in IBD (*41*). As it was reported that protein kinase A (PKA), protein kinase C (PKC), and protein kinase G (PKG) regulate cellular processes in diarrhea (*42*–*44*), we treated colonoids with corresponding agonists for each of these kinases (Forskolin for PKA; PMA for PKC; 8-br-cGMP for PKG). Colonoids treated with forskolin (*45*), but not PMA or 8-br-cGMP, showed robust swelling (Fig. 4A). We then treated colonoids with four chemically distinct PKA inhibitors (SQ-22536 and KH 7 target adenylyl cyclase, the upstream of PKA; H-89 and A-674563 target PKA) and observed that all four inhibitors inhibited the iIAF-CM–induced colonoid swelling and leakage (Fig. 4, B and C, and fig. S4, A and B). These results suggest that iIAF-induced colonoid swelling is PKA dependent.

Transepithelial fluid secretion is associated with activation and deactivation of ion channels (*46*), which may act downstream of PKA. In the colon, absorption of water is mostly regulated by sodium transporters, including sodium-hydrogen exchanger 3 (NHE3) and epithelial sodium channel (ENaC) (*43*). We treated colonoids with iIAF-CM in combination with inhibitors of each (Tenapanor for NHE3 and Benzamil for ENaC). Only Benzamil reduced colonoid swelling, but not significantly (Fig. 4D and fig. S4, C and D). This suggests that iIAF-CM–induced colonoid swelling was not dependent on sodium absorption. Colon epithelial fluid secretion is known to be mostly regulated by chloride channels, namely, the cystic fibrosis transmembrane conductance regulator (CFTR) and the calcium-dependent chloride channel (CaCC) (*43*). We therefore treated colonoids with inhibitors against each [CFTR(inh)-172 for CFTR and the general TMEM16 family inhibitor, CaCC(inh)-A01 for CaCC]. Only the CFTR inhibitor prevented iIAF-CM–induced colonoid swelling (Fig. 4D and fig. S4D), suggesting that CFTR but not members of the calcium-dependent TMEM16 family was involved in this regulation. CFTR is a known target of PKA activation (*47*). Thus, iIAF-induced organoid swelling is mediated through the PKA-CFTR axis.

### iIAF-induced colonoid swelling occurs downstream of $PGE_2$-EP4 signaling

Next, we investigated the signaling pathway upstream of PKA. Many factors can activate PKA in the context of diarrhea, including small molecules, cytokines, and neurotransmitters (*44*). To probe the molecular nature of the paracrine agent, we fractionated the CM using filters of 3-kDa molecular weight (MW) cutoff (MWCO) and treated colonoids with the top (MW > 3 kDa) and bottom (MW < 3 kDa) fractions (Fig. 5A). The bottom fraction from iIAF-CM induced colonoid swelling more robustly than the top fraction (Fig. 5A), suggesting that the major agent inducing colonoid swelling was likely to be a small molecule.

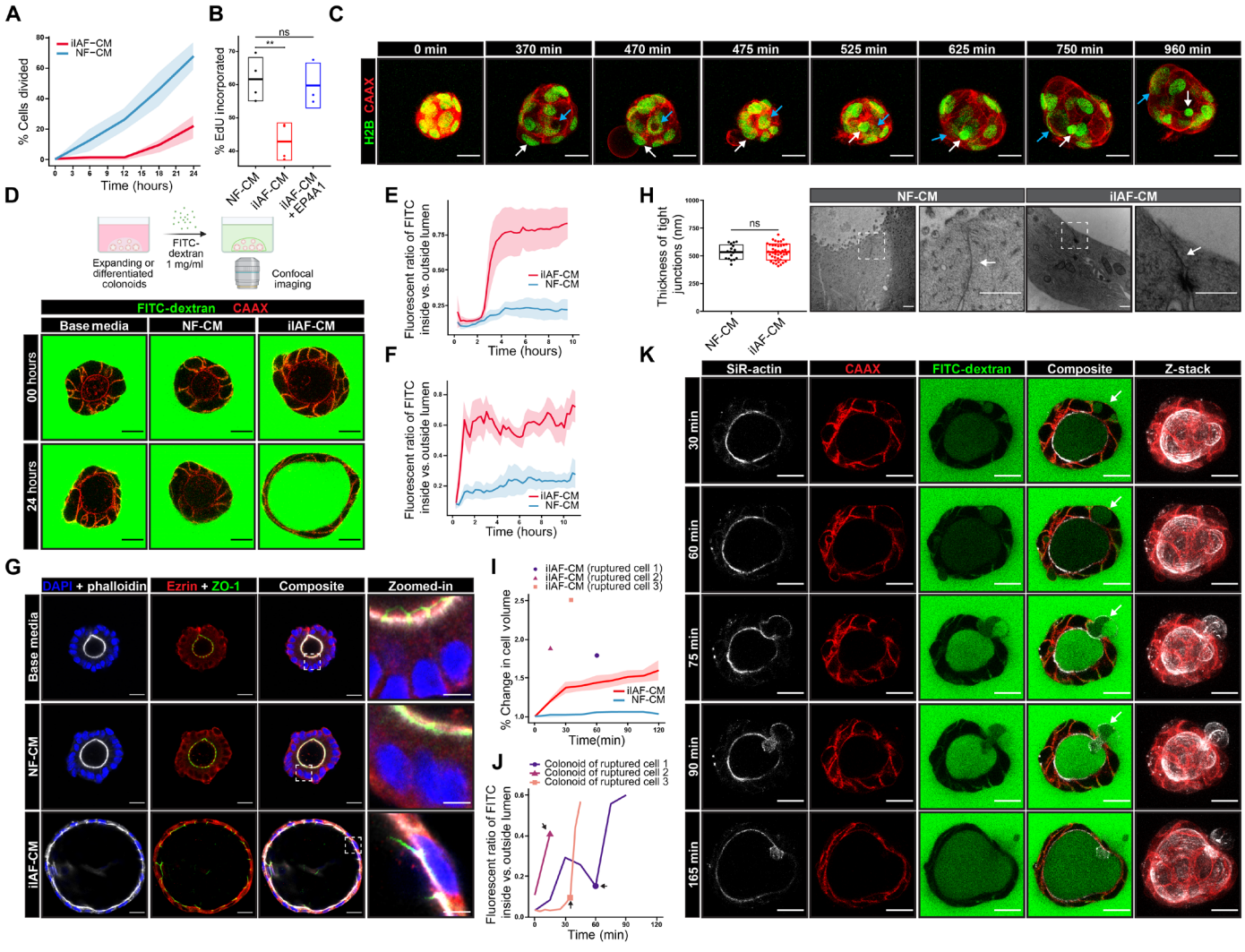


**Fig. 3. Barrier disruption and cell rupture are observed in iIAF-induced colonoid swelling.** (**A**) iIAFs suppress colonoid proliferation. Solid line represents the mean and shaded area represents SEM, which also applies to (E), (F), and (I). (**B**) iIAFs inhibit EdU incorporation in colonoids. Bar box represents mean ± SD. (**C**) iIAF-CM induces both colonoid swelling and cell swelling. White arrows point to an individual cell that underwent swelling and rupture over time. Blue arrows point to another cell that formed a large intracellular vacuole. (**D**) iIAF-CM increases the permeability of colonoids. Top: Schematic representation of the workflow used to examine colonoid barrier function. Bottom: Representative images showing that iIAF-CM increases permeability of colonoids. Scale bar, 20 μm. (**E**) iIAF-CM increases the permeability of expanding colonoids. (**F**) iIAF-CM increases the permeability of differentiated colonoids. (**G**) iIAF-CM cultured colonoids retain tight junctions and polarity. Representative immunofluorescent images of colonoids cultured in NF-CM or iIAF-CM. Scale bars, 20 and 5 μm in original and zoomed-in images, respectively. (**H**) iIAF-CM does not affect intercellular thickness of tight junctions. Left: Box plots showing the intercellular thickness of tight junctions. Right: Representative TEM images of colonoid treated with iIAF-CM or NF-CM. White arrows indicate tight junctions. Scale bar, 500 nm. (**I**) iIAF-CM increases cell volume and causes rupture in some cells. Line shows the change in volume over time of individual cells in colonoids treated with iIAF-CM or NF-CM. Circle, triangle, and rectangle symbols represent three iIAF-CM cultured cells that ruptured. (**J**) iIAF-CM–induced cell rupture is associated with barrier disruption. The circle, triangle, and rectangle represent the corresponding cells and time point of cellular rupture described in (I). (**K**) iIAF-CM induces colonoid swelling, rupture, and barrier disruption. Images show the time course of a colonoid cell (white arrow) that swelled and eventually ruptures.

Because most small molecules activate PKA through G protein–coupled receptors (GPCRs) (*48*), we considered potential GPCR activators associated with inflammation. Among them, prostaglandins are intermediate products from the arachidonic acid (AA) pathway under the regulation of cyclooxygenase (COX) (*49*), and their production and secretion in IAFs are up-regulated upon inflammation in IBD patients (fig. S5, A and B) (*50*, *51*). To examine whether prostaglandins were involved in organoid swelling, we first confirmed increased *PTGS1/2* (encoding COX1/2) expression in IL4 + IL13 + TNFα–activated iIAFs (Fig. 5B). We then treated iIAFs with COX inhibitors [including Rofecoxib, Lornoxicam, S-Ibuprofen, SC-560, and 5-aminosalicylic acid (5-ASA)] during iIAF induction and collected iIAF-CM for colonoid culture. Colonoids treated with COX-inhibited iIAF-CM did not swell (Fig. 5C).

Prostaglandin $E_2$ ($PGE_2$) is the most abundant type of prostaglandin in the colon (*52*). We performed enzyme-linked immunosorbent assays (ELISAs) on iIAF-CM derived from multiple

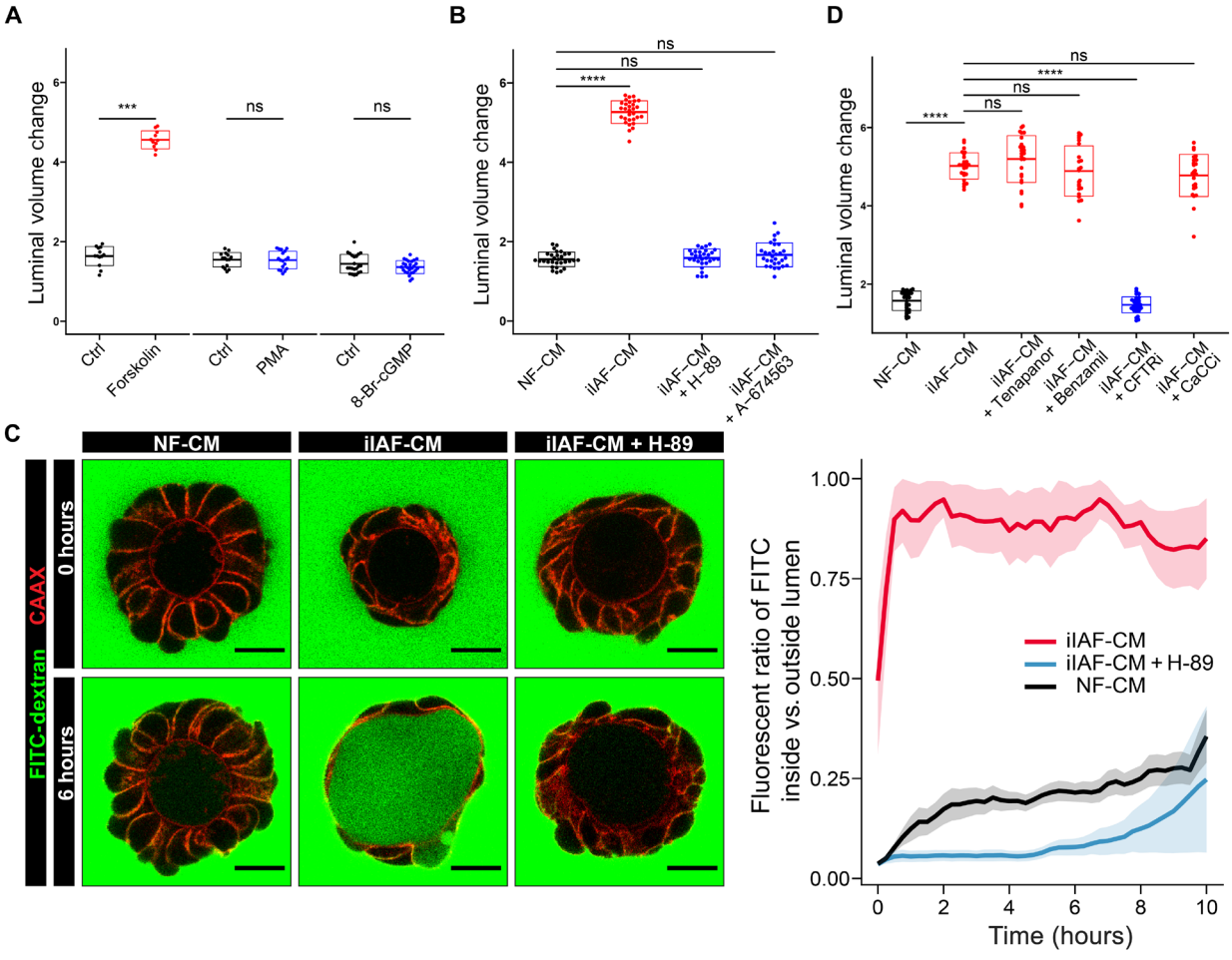


**Fig. 4. iIAFs induce colonoid swelling through PKA-CFTR signaling.** (**A**) Colonoid swelling can be induced by PKA activation. Box plots show luminal volume changes of colonoids treated with PKA, PKC, and PKG agonists (Forskolin, PMA, and 8-Br-cGMP), respectively. Bar box represents mean ± SD. (**B**) PKA inhibitors prevent iIAF-CM–induced colonoid swelling. Box plots show luminal volume changes of colonoids cultured in iIAF-CM with or without PKA antagonists H-89 and A-674563. Bar box represents mean ± SD. (**C**) PKA inhibitors prevent iIAF-CM–induced barrier leakage. Left: Representative live images of colonoids treated with NF-CM, iIAF-CM, and iIAF-CM with PKA inhibitor, H-89, in an FITC-dextran permeability assay. Images shown are at the beginning of and 6-hour time point after culturing in CM. Scale bar, 20 μm. Right: Line plot showing the fluorescence ratio of FITC inside versus outside the lumen, with six, six, and three organoids quantified for NF-CM, iIAF-CM, and iIAF-CM + H-89, respectively. The lines show the mean and the shaded areas show the SEM. (**D**) iIAF-CM–induced colonoid swelling is CFTR dependent. Box plots show luminal volume changes of colonoids cultured in iIAF-CM with Tenapanor (NHE3 inhibitor), Benzamil (ENaC inhibitor), CFTR inhibitor-172 (CFTR inhibitor), or CaCC(inh)-A01 (TMEM16A family inhibitor), respectively. Three independent experiments were performed with consistent results. Data shown are from a single independent experiment, with 30 colonoids measured per condition. Bar box represents mean ± SD.

fibroblast cell lines (normal and IBD-derived) and found that the level of $PGE_2$ was significantly increased in all compared to the NF-CM controls (Fig. 5D). Treating multiple colonoid lines with $PGE_2$ led to increased luminal volume (Fig. 5E) in a dose-dependent manner (fig. S5C). Additionally, treating colonoids with $PGE_2$ reduced EdU incorporation, suggesting that $PGE_2$ contributed to the observed reduction of epithelial proliferation in iIAF-colonoid cocultures (fig. S5D). The same effect is also observed in CM derived from IL1β + TNFα–activated iIAFs (fig. S5, E and F). Next, to examine whether $PGE_2$ was sufficient to induce colonoid swelling at the concentration present in iIAF-CM, we treated colonoids with a matched concentration of $PGE_2$ as measured by ELISA in iIAF-CM and found no statistical difference of luminal volume increase induced by iIAF-CM or by $PGE_2$ at the matched concentration (Fig. 5F).

Four GPCRs are known as $PGE_2$ receptors, namely, EP1, EP2, EP3, and EP4 (*53*). Among these, EP1 is a $Ga_q$- that activates PI3K-dependent pathways (*53*). EP2 and EP4 are coupled to $Ga_s$ and activate adenyl cyclase (*54*). Although both EP2 and EP4 signal through PKA, EP4 also utilizes the PI3K pathway and activates ERK1/2 (*55*). EP3 is a PKA inhibitor and not detected in colon epithelium (*56*). Because PTGER1 and 4 (corresponding to EP1 and EP4 respectively) are up-regulated in inflamed epithelial cells in IBD patients (fig. S5G), we treated colonoids with $PGE_2$ in combination with distinct EP1 or EP4 antagonists [ONO-8130 and sc-51089 for EP1; E7046 and EP4 receptor Antagonist 1 (EP4A1) for EP4] (Fig. 5G and fig. S5H). We observed that EP4 inhibitors prevented colonoid swelling but EP1 inhibitors did not (Fig. 5G and fig. S5F). Because both EP2 and EP4 could activate cAMP (*54*), we treated colonoids with selective EP2 and EP4

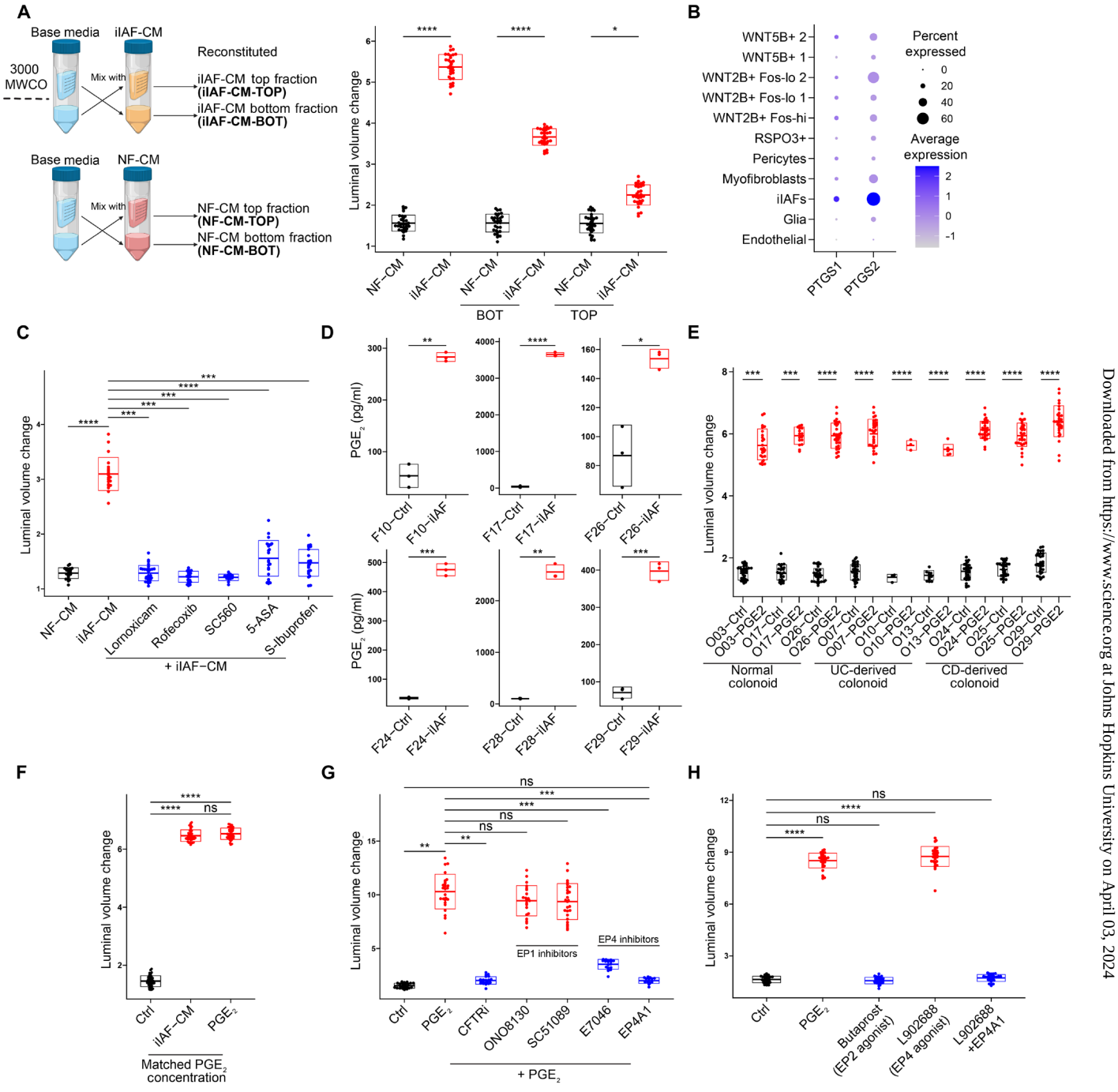


**Fig. 5. iIAFs secrete $PGE_2$ and induce colonoid swelling through EP4.** (**A**) Small molecules in iIAF-CM induce colonoid swelling. Left: Schematic representation of the workflow used to generate fractionated CM for colonoid culture. CM (10 ml) was fractionated into 1 ml of concentrated (top) and 9 ml of flowthrough (bot) fractions and mixed with the complementary fractions from the base media (crossing arrows). Right: Box plots showing the luminal volume change of colonoids cultured in top or bottom fractions of iIAF-CM and NF-CM. Bar box represents mean ± SD. (**B**) *PTGS1/2* are up-regulated in iIAFs. Dot plot shows the expression of *PTGS1/2* (encoding COX1/2) in different subsets of patient-derived fibroblasts. (**C**) CM from COX inhibitor-treated iIAFs does not induce colonoid swelling. Box plot shows the luminal volume changes of colonoids cultured in iIAF-CM that is derived from iIAFs pretreated with COX inhibitors during cytokine-activation. COX inhibitors were washed out before generating CM. Bar box represents mean ± SD. (**D**) $PGE_2$ is up-regulated in multiple iIAF lines. Box plots show the $PGE_2$ concentration of iIAF-CM derived from six iIAF lines using a $PGE_2$ ELISA. Bar box represents mean ± SD. (**E**) $PGE_2$ induced colonoid swelling in multiple colonoid lines. Box plot shows luminal volume changes of nine colonoid lines cultured in 10 nM $PGE_2$. (**F**) $PGE_2$ is the factor in iIAF-CM responsible for colonoid swelling. Box plot shows luminal volume changes of colonoids cultured in iIAF-CM or $PGE_2$ at a concentration matched with the $PGE_2$ concentration in iIAF-CM (measured 2116.70 pg/ml, approximately 6.01 nM by ELISA). (**G**) $PGE_2$-induced colonoid swelling is EP4 dependent. Box plots show luminal volume changes of colonoids cultured in $PGE_2$ with different EP1 and EP4 inhibitors. Bar box represents mean ± SD. (**H**) EP2 is not involved in $PGE_2$-induced colonoid swelling. Box plots show luminal volume changes of colonoids cultured in EP2 or EP4 agonists. Bar box represents mean ± SD.

agonists (Butaprost and L-902688, respectively) and observed that only the EP4 agonist induces organoid swelling (Fig. 5H and fig. S5I). These data show that iIAF-induced colonoid swelling is mediated by $PGE_2$ activation of EP4.

Last, to determine whether $PGE_2$ signaling was sufficient to cause epithelial barrier disruption, we treated colonoids with 10 nM $PGE_2$, a concentration at the higher end among different batches of iIAF-CM (Fig. 5D and fig. S5J). The $PGE_2$-treated colonoids showed increased luminal FITC-dextran leakage, which was rescued by an EP4 inhibitor (fig. S5J). Treating colonoids with iIAF-CM showed slightly higher permeability than matched $PGE_2$ (fig. S5K). These data suggest that $PGE_2$ is critical for the IAF-induced barrier disruption phenotype, but additional factors may also be involved (*57*) (fig. S5L).

### iIAF-induced colonoid swelling increases DNA damage and mitotic errors that are mitigated by EP4 inhibition

Because rapid changes in osmotic or mechanical stress can increase DNA damage and compromise mitotic fidelity (*58*–*62*), we hypothesized that iIAF-induced epithelial swelling, which markedly alters cell and nuclear shape, could increase mitotic errors and DNA damage, which are causes of CIN associated with CAC initiation and progression (*63*). To test this, we first monitored cell divisions by live-cell imaging using normal colonoids expressing both H2B-mNeonGreen and mCherry-CAAX. Colonoids treated with iIAF-CM showed increased mitotic errors, including chromosome bridges and lagging chromosomes (Fig. 6, A and C). To confirm that this phenotype can be caused by $PGE_2$ signaling, we treated colonoids with 10 nM $PGE_2$ and observed a similar increase in mitotic errors (Fig. 6B). Time-lapse imaging of $PGE_2$-treated colonoids showed many examples of grossly misaligned chromosomes during mitosis of swollen and distorted epithelial cells (Fig. 6D, fig. S6A, and movies S4 and S5). Additionally, 53BP-1, a marker of the DNA damage response, accumulated and persisted at sites where chromatin bridges were severed during cytokinesis (Fig. 6E and movies S6 and S7). Immunofluorescent staining of colonoids with γH2AX, a marker of double-stranded DNA breaks, confirmed increased DNA damage in both iIAF-CM and $PGE_2$-treated colonoids compared to controls in both dividing and differentiated cell types (Fig. 6, F and G, and fig. S6B).

To evaluate whether mitotic errors led to aneuploidy, we performed chromosome counting using metaphase spreads (fig. S6C). We observed a significant increase in aneuploid and tetraploid cells in colonoids treated with IAF-CM (Fig. 6H and fig. S6D). Similar results were observed when treating colonoids with $PGE_2$ (Fig. 6I and fig. S6E). Live cell imaging revealed that tetraploidy can arise from failed cytokinesis, which could be disrupted due to cell swelling (Fig. 6J). We observed the formation of large intracytoplasmic vacuoles (>5 μm) that displaced cytoplasmic contents (fig. S6, F and G, and movies S3 to S5) in swollen epithelial cells, which could also interfere with cell division. Treating colonoids with an EP4 inhibitor prevented both increased DNA damage and the induction of aneuploidy and tetraploidy caused by iIAF-CM or $PGE_2$ (Fig. 6, F to I). Thus, iIAF-induced colonoid swelling is a source of genome instability that can be mitigated by EP4 inhibition.

## DISCUSSION

Although numerous studies have implicated IAFs in IBD pathogenesis, none have directly queried the interaction between IAFs and colon epithelium and how and whether they contribute to colitis-associated epithelial biology (*15*, *22*, *64*, *65*). Here, we develop an in vitro method of coculturing human colon–derived IAF and colon epithelium to investigate the role of IAFs in instigating and perpetuating epithelial dysfunction relevant to IBD biology. Using scRNA sequencing, live cell imaging, and biochemical assays, we found that IL4 + IL13 + TNFα–induced fibroblasts recapitulate key features of IAFs in vivo. These cytokine-activated IAFs cause colonoid swelling and barrier disruption in a PKA- and CFTR-dependent manner downstream of $PGE_2$-EP4 signaling. IAF-induced epithelial swelling leads to DNA damage and mitotic errors, which can be mitigated by inhibiting the $PGE_2$ receptor EP4. Our findings thus shed light on the cellular and molecular mechanism of IAFs and the importance of prostaglandin signaling in IBD pathogenesis.

Because of the complex and multifactorial nature of IBD, we used colonoids, an in vitro three-dimensional cell culture system in Matrigel, to focus on the direct impact of IAFs on the function and integrity of epithelial cells. As both $T_H1$ and $T_H2$ responses drive IBD pathogenesis (*25*), our results accordingly show that $T_H1$- and $T_H2$-associated cytokines can convert NFs into IAF-like cells. These iIAFs have transcriptional nuances that may be reflective of IBD disease stage; for example, we show that iIAFs induced by $T_H1$ cytokine IL1β + TNFα showed signatures of chemotaxis (Fig. 1, K and L), whereas IAFs induced by $T_H2$ cytokines IL4 + IL13 + TNFα showed increased ECM signatures (Fig. 1, K and L), as described in IBD-derived IAFs previously (*15*). Although $T_H2$ cytokines IL4 and IL13 are generally associated with tissue repair (*66*), studies have shown that their uncontrolled expression can be proinflammatory (*67*, *68*) and associated with fibrosis in IBD (*69*, *70*). Recent murine studies also suggest that $T_H2$ cytokine expression is up-regulated in late-stage colitis models (*25*, *70*). Together, our data and these findings informed our choice of IL3, IL4, and TNF-α as the cytokines used experimentally for IAF induction.

Although up-regulation of $PGE_2$ in IBD tissue has been recognized for decades (*71*, *72*), its major cellular source and role have been unclear and even controversial. Previous studies have reported macrophages, monocytes, mesenchymal stem cells, and T cells as putative sources of $PGE_2$ (*73*–*77*). However, none of those cell types alone produce the same level of $PGE_2$ measured in IBD patients (*78*, *79*). Our data show that iIAFs can produce nanomolar concentrations of $PGE_2$, suggesting that they may be a major source of $PGE_2$ in IBD. Regarding the function of $PGE_2$, previous studies in IBD suggest that $PGE_2$ can be both pro-inflammatory and anti-inflammatory in the context of different recipient cells (*74*–*77*, *80*, *81*). Our data suggest that $PGE_2$ has a pro-inflammatory role in the context of epithelial cells, leading to epithelial swelling, crypt distortion, disrupted barrier function, mitotic errors, and DNA damage. In addition to IBD, IAFs and $PGE_2$ are also associated with other chronic inflammatory diseases such as idiopathic pulmonary fibrosis (*82*), rheumatoid arthritis (*83*), and chronic kidney disease (*84*). The pathway that we have identified may help explain the role of IAFs in the pathogenesis of these diseases.

$PGE_2$ is known to promote isosmotic fluid secretion by stimulating chloride secretion while blocking sodium absorption (*85*). This action is accompanied by water secretion across the epithelium. Our results show that tight junctions were overall intact during iIAF-induced colonoid swelling, suggesting that fluid flow was trans-cellular rather than intercellular. This is consistent with our observation that individual cells in colonoids could swell when exposed to iIAF-CM. Cell swelling is likely to be a consequence of unbalanced or uncoordinated fluid influx versus efflux. Although this swelling phenomenon may manifest

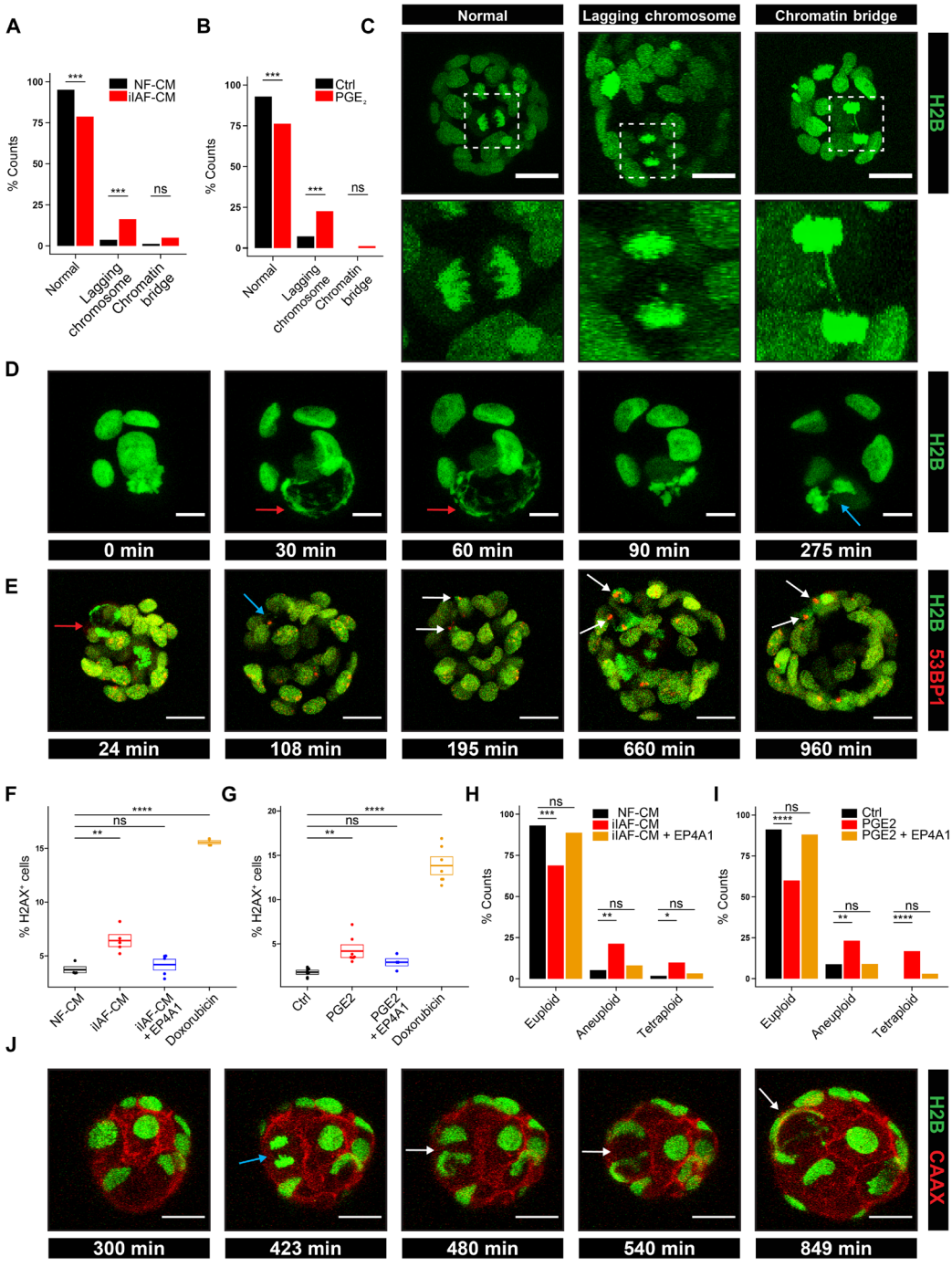


**Fig. 6. $PGE_2$ negatively affects mitotic fidelity and increases DNA damage.** (**A**) Colonoids exhibit increased mitotic errors when cultured in iIAF-CM. Fisher's exact test. (**B**) Colonoids exhibit increased mitotic errors when cultured in $PGE_2$. Fisher's exact test. (**C**) Colonoids undergoing normal or erroneous mitoses. Representative images of colonoid cells undergoing mitosis with chromatin bridge, lagging chromosome, or normal mitosis. Scale bar, 20 μm. (**D**) Swelling of individual colonoid cells affects mitosis. Representative live cell images showing a cell in a colonoid in M phase at the beginning of $PGE_2$ treatment. $PGE_2$-induced cell swelling disrupted alignment of chromosomes (red arrows) and led to erroneous mitosis (blue arrow). Scale bar, 10 μm. (**E**) Mitotic errors are a cause of DNA damage in colonoids. Representative live cell images showing that mitotic errors led to DNA damage. The red arrow shows a $PGE_2$-treated dividing cell with a chromatin bridge that led to DNA damage (blue arrow). 53BP1 foci persisted for more than 12 hours (white arrows). Scale bar, 20 μm. (**F**) iIAF-CM increases the incidence of DNA damage in colonoids. Bar box represents mean ± SD. (**G**) $PGE_2$ increases the incidence of DNA damage in colonoids. Dot plot shows the percentage of H2A.X-positive cells after 6 hours of 10 nM $PGE_2$ treatment. Bar box represents mean ± SD. (**H**) iIAF-CM–treated colonoids have more aneuploidy and tetraploidy. Fisher's exact test. (**I**) $PGE_2$-treated colonoids have more aneuploidy and tetraploidy. Box plot shows the percentage of chromosome counts of colonoids treated with base media (control), $PGE_2$, or $PGE_2$ + EP4A1 in the metaphase chromosome spread assay. Fisher's exact test. (**J**) $PGE_2$ induces tetraploidy via cytokinesis failure. Representative live cell images of a colonoid cell that underwent normal metaphase (blue arrow) but failed cytokinesis (white arrows). Scale bars, 20 μm.

differently in vitro compared to in vivo, the rapid influx of fluid into the luminal space of the epithelium is physiologically analogous to what happens in diarrhea, a symptom affecting most IBD patients (*41*). While most cells in colonoids did not undergo marked swelling, even one or few cells in a colonoid undergoing marked swelling and rupture could lead to local disruption of epithelial barrier, as shown by live imaging. In mitotic cells that underwent swelling, the spindle and chromosome alignment appeared grossly abnormal, leading to segregation defects and DNA damage. This may be consistent with previous reports that cell compression and shape distortion disrupt spindle morphogenesis and lead to mitotic errors (*58*, *59*). Additionally, DNA damage can occur when the nucleus is compressed or distorted (*60*, *62*). We observed many cases in live-cell imaging assays where cell nuclei are flattened or deformed into lobular shapes (fig. S6G).

Our study provides insights into the association of persistent IAFs and treatment-refractory IBD. We show that multiple cytokine cocktails, even without TNFα, can lead to varying IL13RA2 expression and IAF phenotypes (Fig. 1D). Thus, resilience of the IAF phenotype in the setting of variable cytokine milieus and pharmacologic TNFα blockade could contribute to heterogeneity of patient disease trajectories and treatment responses. For example, IL1β + TNFα–activated iIAFs showed stronger chemotaxis-associated signatures (Fig. 1, K and L), which could promote more robust immune infiltration into the lamina propria. These data highlight the potential value of combinatorial immunomodulatory therapeutic approaches in IBD.

Another potentially translatable finding of our study is that EP4 is a critical mediator of the iIAF-epithelial interaction. Mutations in the EP4 encoding gene *PTGER4* are associated with both UC and CD in a genome-wide association study (*86*). We found that blocking EP4 prevents iIAF-induced epithelial swelling, barrier disruption, DNA damage, and mitotic errors. Others have suggested a role for EP4 antagonists in modulating regulatory T cells and gut microbiome in chronic intestinal inflammation (*84*). Our data identify another key role for $PGE_2$-EP4 antagonism in promoting epithelial homeostasis. As such, EP4 antagonists may be useful therapeutic agents to treat both acute and chronic sequelae of IBD. To date, EP4 antagonists have not been used in IBD-associated clinical trials but are under active clinical trials for treating solid tumors in combination with PD-1 blockades. Several of these trials have completed dose escalation and have entered phase 1b (NCT04443088) or phase 2 (NCT02538432, NCT03696212), suggesting that these agents may be exploited for promoting epithelial barrier integrity and mitigating CAC risk.

Although our study provides a mechanistic understanding of how human IAFs affect colon epithelium in vitro using patient-derived fibroblasts and colonoids, our study was not extended to observing their interactions directly in vivo. However, in a previous report, knocking out *Ptgs2* (encoding *COX2*) in fibroblasts reduced the level of $PGE_2$ in mice and prevented tumor initiation in the azoxymethane (AOM) colon cancer model (*80*). Our results provide a possible explanation for this observation in a patient-derived culture system. We also note that EP4 was reported to suppress TNFα-induced intestinal epithelial necroptosis by inhibiting MLKL oligomerization and membrane translocation (*87*), suggesting that $PGE_2$ signaling has multiple roles in IBD.

## MATERIALS AND METHODS

### Patient sample collection

Fresh colonic tissue was harvested from patient specimens (CD, UC, and unaffected normal) within 30 min of surgical resection, with informed consent under approved Johns Hopkins School of Medicine Institutional Review Board protocol IRB00125865. All specimens were carefully evaluated, annotated, and harvested by an expert gastrointestinal pathologist (T.L.). Clinical information and metadata are summarized in table S1. A corresponding formalin-fixed paraffin-embedded (FFPE) sample was taken for each fresh sample for histological evaluation (table S1). Fresh samples were immediately placed into complete Dulbecco's Modified Eagle Medium [DMEM; 10% heat-inactivated fetal bovine serum (HI-FBS) + 1× antibiotic-antimycotic in DMEM high glucose] and transported at 4°C.

### Colonoid and fibroblast line generation

Samples were transported to the laboratory within 1 hour of surgical resection. They were briefly washed in ice-cold phosphate-buffered saline (PBS) containing 1× penicillin/streptomycin (Pen/Strep) and trimmed into smaller pieces (<1 $mm^2$). Samples were washed extensively using ice-cold Hanks' balanced salt solution (HBSS) until the supernatant turned clear. For postprocessing, most surgical samples were immediately stored in 90% HI-FBS + 10% dimethyl sulfoxide (DMSO) and cryopreserved in liquid nitrogen. The remaining samples were used to generate colonoids and/or fibroblasts.

For colonoid generation, samples were transferred into a 50-ml conical tube containing 10 ml of stripping buffer (5 mM EDTA + 1× Pen/Strep +2% FBS + 1× Hepes in HBSS without $Ca^{2+}$/$Mg^{2+}$). Sample pieces were shaken on an orbital shaker at 37°C for 20 min at 200 rpm to release crypts. Released crypts were collected to generate colonoid lines as previously described (*37*).

For fibroblast isolation, minced tissue was transferred into a 50-ml conical tube containing 10 ml of digestion buffer [Liberase (0.05 mg/ml) TH + 1× Pen/Strep +2% FBS + 1× Hepes in HBSS with $Ca^{2+}$/$Mg^{2+}$]. Sample pieces were shaken on an orbital shaker at 37°C for 60 min at 200 rpm. Then, digested cells were filtered through a 40-μm strainer and centrifuged at 200*g* for 5 min at 4°C. After removing the supernatant, red blood cells were removed by adding 2 ml of ACK lysis buffer for 2 min at room temperature (RT) followed by another round of centrifugation. Last, cells were resuspended in cDMEM and seeded in six-well plates at 2 million cells/ml. Forty-eight hours after seeding, the media was changed to remove both dead and suspension cells. The media was then changed once every 3 days and cells were passaged when they reached 90% confluency. Bulk fibroblast lines were established at approximately passage 4, confirmed by scRNA-seq (in other words, non-fibroblast cell populations were not recovered using unbiased cell mapping approaches). Fibroblasts were maintained in T75 flasks and passaged at a 1:3 to 1:4 ratio every 5 days. These primary fibroblasts can be maintained for at least 15 passages without apparent changes to proliferation rate. All fibroblasts used for experiments were within the first 10 passages.

### Single-cell RNA sequencing of patient-derived fibroblast lines

For fibroblast scRNA-seq experiments, the Chromium Next GEM single cell 3' HT reagent kit V3.1 was used for sample preparation. After QC, sequencing was performed using an S4 flow cell in a NovaSeq 6000 system. The targeted read depth was 50 K reads per cell and 2 K reads per cell multiplexing oligo barcode. After sequencing, data were uploaded to the 10x cloud analysis server and analyzed using Cell Ranger 7.0.1. Further analysis was performed in R (4.3.0) using Seurat (4.2.0), monocle3 (1.3.1), followed by the standard data processing and analysis workflow.

Reference mapping was performed using a slightly modified protocol from the original publication (***29***). In brief, Seurat objects were normalized using SCTransform and anchors were calculated using the standard principal component analysis transformation (UCatlas as reference and our fibroblast cell dataset as the query dataset) to find and transfer matched cell-type labels. Then, the query dataset was projected onto the Uniform Manifold Approximation and Projection (UMAP) structure.

Wilcoxon rank-sum test was used to find markers for each subset. To compare the DEGs between IL1β + TNFα IAFs versus IL4 + IL13 + TNFα IAFs, pseudobulk analysis was performed in Libra (*88*), using the edgeR (3.17) LRT method. GSEA was performed using rankings and annotated using org.Hs.eg.db (3.17.0).

## Colonoid related culture methods

### *General colonoid culture*

Colonoids were cultured and passaged in organoid expansion media (including EGF, Wnt3A, R-spondin1, and Noggin, aka EWRN media). For the first 3 days after seeding, 10 μM Y-27632 was added to avoid anoikis. Then, expansion media was changed once every 2 days and colonoids were passaged weekly. For all experiments, colonoids were used before passage 25. Experiments with expanding colonoids were performed on day 4 after single-cell seeding. All small-molecule drugs were reconstituted in DMSO and stored at −20°C. Unless otherwise specified, the concentration of the chemicals was as follows: Forskolin (10 μM), H-89 (50 μM), A-674563 (10 μM), Tenapanor (10 μM), Benzamil (10 μM), CFTRi (10 μM), CaCCi (10 μM), $PGE_2$ (10 nM), ONO8130 (10 μM), SC51089 (10 μM), E7046 (50 μM), EP4A1 (10 μM), Butaprost (10 nM), L902688 (10 nM), and Doxorubicin (0.5 nM).

### *Colonoid differentiation*

For experiments using differentiated colonoids, colonoids were switched to differentiation media (expansion media without Wnt3A and SB202190, a p38 inhibitor) on day 4 after single-cell seeding and maintained for 4 additional days. Media was renewed once every 2 days. Colonoid differentiation was visually confirmed by observation of budding phenotypes, as described previously (*37*).

### *Transwell colonoid-fibroblast coculture*

Colonoids were mixed in 20 μl of Matrigel, seeded in the Transwell (0.4 μm PET membrane; Corning, catalog no. 353095), and settled in a glass-bottom 24-well plate (Cellvis, catalog no. P24-1.5H-N). Expansion media (100 μl and 600 μl) were added into the transwell and the plate, respectively. Colonoids were cultured for 4 days before dissociated fibroblasts were added. Imaging was then performed using the Nikon TiE microscope, as described in the imaging section.

### *Colonoid culture for transmission electron microscopy*

Colonoids were mixed in 10 μl of Matrigel, loaded in a sterilized specimen carrier A (specimen carrier, 6 mm, 0.1/0.2 mm) (Technotrade 1190-100), and cultured in a 24-well plate for 4 days. Expansion media was then switched to fibroblast CM for 6 hours followed by high-pressure freezing, as described in the High-pressure freezing and freeze substitution section.

## Fibroblast related culture methods

### *Cytokine induction*

Fibroblasts were seeded at about 20% confluency. Two days after seeding, fibroblasts were treated with cytokines for 4 days. Then, cells were collected for downstream assays, including Western blot, coculture, and CM generation. For cytokine induction, unless otherwise stated, all cytokines were reconstituted as 1,000× working stocks in cDMEM at 10 μg/ml except TNFα (50 μg/ml) and stored at −20°C before use.

### *Generation of fibroblast CM*

After cytokine induction by IL4 + IL13 + TNFα, fibroblasts were washed three times in PBS to remove remaining cytokines and supplied with organoid culture media (expansion or differentiation media) for 1 day. CM was then collected and centrifuged at 600*g* for 5 min to remove cell debris. CM was stored at −20°C for long-term storage and at 4°C for immediate use within a week.

### *Generation of COX inhibitor-treated iIAF-CM*

During cytokine induction, COX inhibitors were added together with IL4 + IL13 + TNFα. Then, drugs were washed away, and CM was generated using the same approach as described above. COX inhibitors were reconstituted in DMSO and stored as 1,000× working stocks at −20°C before use. The default working concentrations of each were as follows: Lornoxicam (50 μM), Rofecoxib (50 μM), S-Ibuprofen (50 μM), SC-560 (50 μM), and 5-ASA (200 μM).

## Ultrafiltration

Ultrafiltration was performed using a 3000 MWCO PES concentrator (Pall Lab, catalog no. MAP003C36). Media (10 ml) was loaded to the concentrator and centrifuged at 5,000*g* for 2 hours at 4°C to generate an approximately 1-ml concentrated fraction (top fraction) and a 9-ml flowthrough fraction (bottom fraction). After ultrafiltration, the concentrated fraction (top fraction) of the CM was reconstituted with the flowthrough fraction (bottom fraction) of the base media; the flowthrough fraction (top fraction) of the CM was reconstituted with the concentrated fraction (bottom fraction) of the base media.

## Confocal imaging

Confocal imaging was performed using a Zeiss LSM880-Airyscan FAST microscopy equipped with an incubation chamber. Colonoids were seeded on eight-well chambered coverglass (Nunc LabTek II, catalog no. 155360 or ibidi, catalog no. 80827) and imaged 4 days after single-cell seeding. For live-cell imaging, cells were incubated at 37°C with 5% $CO_2$ and imaged using a 40×/1.20 C-Apo water objective with Zeiss Immersion Oil W 2010 media. For cell division assays, colonoids were imaged once every 3 min with 30 to 50 1.0- to 1.5-μm z-slices. For FITC-dextran permeability assays, colonoids were imaged once every 15 min with 30 to 40 1.5- to 2.0-μm z-slices. For fixed cell imaging, the airyscan mode was used with default settings (zoom factor = 2.0, 40× water objective for proliferating colonoids and 20× air objective for differentiated colonoids). Images were analyzed using ImageJ (version 1.53C).

## Imaging and quantification of colonoid swelling

The colonoid swelling assay was performed using a Nikon TiE microscope equipped with an incubation chamber (37°C, 5% $CO_2$). Colonoids were cultured in 24-well glass bottom black plates (Cellvis, catalog no. P24-1.5H-N) for 4 days and imaged using a 10× objective. Once the areas of interest were selected (three areas per well, each with dimensions of 1311.20 μm × 1328.60 μm), culture media was changed to designated media and imaged every 15 min for 12 to 48 hours. Images were analyzed using ImageJ. The level of swelling was quantified by comparing the fold change of the luminal area before and after the treatment (at 24 hours after treatment, unless

otherwise described). Quantified data were organized and plotted using RStudio (2022.12.0 Build 353).

### Lentivirus production and generation of modified colonoid lines

Lentiviruses were generated using pMD2.G, psPAX2, and corresponding lentiviral transfer constructs. We followed the forward transfection protocol of the Lipofectamine 3000 reagent (Invitrogen, catalog no. L3000008) with some minor changes. In brief, HEK293FT cells were passaged at 1:4 ratio 36 hours before transfection. Cells were cotransfected with the lentiviral transfer plasmid, packaging plasmid (psPAX2), and envelop plasmid (pMD2.G) at a 1:1:1 molar ratio using Lipofectamine 3000 for 6 hours. Then, media containing lentivirus was collected and concentrated 100-fold using the Lenti-X Concentrator (Takara Bio, catalog no. 631231). Lentiviral titers were determined using the qPCR Lentivirus Titration Kit (abm, catalog no. LV900). Lentiviruses were aliquoted into cryogenic tubes (100 μl per tube per transfection), snap frozen in liquid nitrogen, and stored at −80°C.

To generate modified colonoid lines, colonoids were dissociated into single cells and resuspended in 1 ml of colonoid expansion media containing 100 μl of concentrated lentivirus, 10 μM Y-27632, and 0.8 μg/ml polybrene. Single cells were spinfected at RT for 1 hour at 70*g*. Cells were then incubated for 6 hours (37°C, 5% $CO_2$) with gentle agitation once per hour. Last, cells were rinsed with base media and embedded in Matrigel (1000 cells/μl, 20 μl per well in a 24-well plate). Modified colonoids were cultured normally for the first passage. At the beginning of the second passage, puromycin (1 μg/ml) and/or blasticidin (5 μg/ml) was added to media depending on the selection gene(s). For colonoids with some fluorescent reporters, dissociated single-cell colonoids were bulk sorted using a Sony SH800 cell sorter at the end of the third passage to further increase population purity.

### EdU incorporation

Colonoids (4 days after single-cell seeding) were treated with 10 μM EdU for 6 hours before dissociation and staining using the Click-It EdU Alexa Fluor 488 Flow Cytometry Assay kit (Thermo Fisher Scientific, catalog no. C10425).

### Immunofluorescence staining of colonoids (in situ)

Colonoids were washed three times in PBS and fixed in 4% paraformaldehyde for 10 min at 37°C. After fixation, colonoids were washed three times using PBS for 10 min each at RT. Then, colonoids were permeabilized using 0.5% Triton X-100 in PBS for 1 hour at RT and blocked in blocking buffer [10% bovine serum albumin (BSA) + 0.1% Triton X-100 in PBS] for 1 hour at RT. Colonoids were stained with primary antibody in staining buffer (1% BSA + 0.1% Triton X-100 in PBS) at 4°C overnight. After primary antibody staining, colonoids were washed three times in PBS and stained with secondary antibody for 4 hours at RT in staining buffer. Finally, colonoids were washed and left in PBS at 4°C until imaging.

### Western blot

Protein lysis buffer was made fresh before each experiment and kept on ice. Lysis buffer included 142.8 μl of 7× protease/phosphatase inhibitor stock (mixture of Roche, catalog no. 11836153001 and catalog no. 4906845001), 100 μl of 10× radioimmunoprecipitation assay buffer, 50 μl of glycerol, 10 μl of 10% SDS, and 697.2 μl of $ddH_2O$. Colonoids (25 μl per well in 24-well plate) and fibroblasts (150 μl per well in a six-well plate) were collected in 1.5-ml Eppendorf tubes and lysed in protein lysis buffer for 30 min with brief vortexing once every 10 min. Lysed cells were further dissociated by sonication at 70 V for 5 min at 4°C and then centrifuged for 10 min at 4°C at 17,000*g* and supernatant was collected. Protein concentrations were measured using a BCA analysis kit (Thermo Fisher Scientific, catalog no. 23225). After normalizing protein concentration, proteins were mixed with 4× loading buffer and 50 mM DTT.

For Western blots, NuPAGE 4 to 12% Bis-tris gels (10/12/15 wells) and MES-SDS (Thermo Fisher Scientific, catalog no. B000202) running buffer were used with default settings. For protein transfer, the iBlot 2 gel transfer system (Thermo Fisher Scientific, catalog no. IB21001) was used with default settings. For imaging, enhanced chemoluminescence substrate (Bio-Rad, catalog no. 170-5060) was used as the detection reagent and the Odyssey XF imaging system (LI-COR Biosciences) was used to record images. Restore Plus Western blot stripping buffer (Thermo Fisher Scientific, catalog no. 46430) was used for membrane stripping.

### mRNA extraction and qPCR

TRIzol (Thermo Fisher Scientific, catalog no. 15596026) was used to collect mRNA. mRNA was extracted using the RNA Mini Kit (Thermo Fisher Scientific, catalog no. 12183018A) with column DNase treatment (Qiagen, catalog no. 79254). After elution, mRNA concentrations were measured using a NanoDrop and normalized to approximately 125 ng/μl. Reverse transcription was performed using SSIV VILO mater mix (Thermo Fisher Scientific, catalog no. 11756050). The cDNA was diluted 20-fold in $ddH_2O$ and mixed with SYBR Green master mix (QuantaBio, catalog no. 95073-05K) and designated qPCR primers. Each reaction was 10 μl and each test was performed in triplicate. β-actin was used as the control gene and untreated fibroblasts were used as control samples. The delta-delta CT method was used for data analysis and Log2 fold change (Log2FC) was used for data presentation.

### Karyotyping

Colonoids were treated with expansion media containing 10% Colcemid (1 μg/ml) for 8 hours and dissociated into single cells using TrypLE Express. Single cells were resuspended in 6 ml of hypotonic solution (0.56% prewarmed KCl) and incubated in a 37°C water bath for 10 min. Then, cells were prefixed by adding 1.5 ml of fixation buffer (methanol:glacial acetic acid = 3:1) and incubating in a water bath for 5 min. Then, cells were centrifuged at 300*g* at RT for 5 min. After removing the supernatant, cells were fixed in 6 ml of fixation buffer and incubated in a water bath for 10 min. After centrifugation, cells were resuspended in 6 ml of fixation buffer and sent for centrifugation immediately without incubation. Resuspended cells were dropped onto a heat-moisturized imaging slide (two drops per slide) and incubated on a heater for 30 min at 75°C. Last, 20 μl of mounting media with DAPI (4′,6-diamidino-2-phenylindole) was loaded evenly onto the slide and a #1.5 22 × 50 mm cover glass was used to cover the spreads. Spreads were counted using a Nikon TiE microscope 63× oil objective and 1.5× focal reducer. At least 50 counts were recorded per condition.

### Flow cytometry

Cells were filtered and analyzed using the Attune NxT flow cytometer (Thermo Fisher Scientific). Results were further processed using

FlowJo (BD, Version 10) for raw data and flow plots. Statistical analysis was then performed with R (version 4.2.2).

### High-pressure freezing and freeze substitution

Colonoids were cultured in specimen carrier A (specimen carrier, 6 mm, 0.1/0.2 mm) (Technotrade 1190-100) and frozen using a high-pressure freezer (EM ICE, Leica Microsystems). BSA (20%) dissolved in colonoid culture medium was used as cryoprotectant. Specimen carrier A with the cells facing up was mounted in the sample holder and enough cryoprotectant was added to cover the cells. Another specimen carrier with a flat side (specimen carrier, 6 mm, 0.3 mm/flat) (Technotrade 1191-100) was placed on top of the specimen carrier A and a 200-μm spacer ring (Leica) was placed on top. The entire assembly was placed in between the half cylinders and frozen using the high-pressure freezer. Frozen samples were dropped in a liquid nitrogen storage container and transferred to an automated freeze substitution (AFS2. Leica Microsystems) unit, keeping the samples under liquid nitrogen. Freeze substitution was performed using two fixatives, fixative I containing 1% glutaraldehyde (Electron Microscopy Sciences, 16530), 0.1% tannic acid (Sigma, 403040-100G), and fixative II containing 2% osmium tetroxide (Electron Microscopy Sciences, 19132) both prepared in anhydrous acetone. Right after freezing, samples were placed in AFS2, in a universal sample container (Leica Microsystems) containing fixative I, prechilled at −90°C and left at −90°C for 40 hours. After that, samples were washed five times with prechilled acetone (−90°C), 30 min per wash. After the last acetone wash, freeze substitution solution II prechilled inside AFS2 was added to the samples. The following steps were performed to complete the freeze substitution process: −90°C for 41 hours, −90° to −20°C in 14 hours, −20°C for 12 hours, and −20° to 4°C in 2 hours, and samples were held at 4°C until further processing. Sample containers were covered with a clear film to prevent evaporation.

### Sample preparation for electron microscopy

Following freeze substitution, fixatives were washed five times with anhydrous acetone, each wash for 20 min. Epon Araldite (100%) was prepared (Epon 6.2 g, Araldite 4.4 g, DDSA 12.2 g, and BDMA 0.8 ml) (Epon-Araldite kit, Ted Pella, 18028) and 30%, 70%, and 90% dilutions were prepared from 100% Epon with acetone. Samples were infiltrated with 30% and 70% Epon solutions for at least 2 hours and 90% overnight. The following day, samples were transferred to freshly prepared 100% Epon, and Epon solution was changed two times. At the final step, the carriers containing the colonoids were placed at the bottom of a BEEM capsule (Electron Microscopy Sciences, 102096-558) such that the cells were facing up and the capsule was filled with 100% Epon. The samples embedded in Epon were cured at 60°C for 48 hours. After the resin was cured, 70- to 90-nm sections were cut using an ultramicrotome (EM UCT, Leica Microsystems) and collected on a 2 × 1 mm copper slot formvar-coated grid.

### Transmission electron microscopy and image analysis

Samples were imaged on a Hitachi 7600 TEM equipped with an AMT XR80 camera with an AMT capture V6 at 80 kV at typically 30,000× magnification. Intercellular junctions were imaged and analyzed using ImageJ.

### Quantification and statistical analysis

Please refer to figure legends or the corresponding Materials and Methods for the description of sample size and statistical details. Statistical analysis was performed using R-Studio (2022.12.0 Build 353, R version 4.2.2). For all statistical tests, $t$ test is performed unless otherwise stated. For significance, $P < 0.05$ was used as the cutoff to indicate significance. For abbreviations, $^{****}P < 0.0001$, $^{***}P < 0.001$, $^{**}P < 0.01$, $^{*}P < 0.05$; ns, not significant.

## Supplementary Materials

**This PDF file includes:**

Figs. S1 to S6
Table S2
Legend for tables S1
Legends for movies S1 to S7

**Other Supplementary Material for this manuscript includes the following:**

Table S1
Movies S1 to S7

## REFERENCES AND NOTES


1. M. B. Buechler, R. N. Pradhan, A. T. Krishnamurty, C. Cox, A. K. Calviello, A. W. Wang, Y. A. Yang, L. Tam, R. Caothien, M. Roose-Girma, Z. Modrusan, J. R. Arron, R. Bourgon, S. Müller, S. J. Turley, Cross-tissue organization of the fibroblast lineage. *Nature* **593**, 575–579 (2021).
2. N. C. Henderson, F. Rieder, T. A. Wynn, Fibrosis: From mechanisms to medicines. *Nature* **587**, 555–566 (2020).
3. M. B. Buechler, W. Fu, S. J. Turley, Fibroblast-macrophage reciprocal interactions in health, fibrosis, and cancer. *Immunity* **54**, 903–915 (2021).
4. Z. Y. Wong, E. Nee, M. Coles, C. D. Buckley, Why does understanding the biology of fibroblasts in immunity really matter? *PLOS Biol.* **21**, e3001954 (2023).
5. S. A. Eming, P. Martin, M. Tomic-Canic, Wound repair and regeneration: Mechanisms, signaling, and translation. *Sci. Transl. Med.* **6**, 265sr266 (2014).
6. H. H. Uhlig, F. Powrie, Translating immunology into therapeutic concepts for inflammatory bowel disease. *Annu. Rev. Immunol.* **36**, 755–781 (2018).
7. C. A. Rubio, P. T. Schmidt, C. Lang-Schwarz, M. Vieth, Branching crypts in inflammatory bowel disease revisited. *J. Gastroenterol. Hepatol.* **37**, 440–445 (2022).
8. S. Danese, C. Fiocchi, Ulcerative colitis. *N. Engl. J. Med.* **365**, 1713–1725 (2011).
9. H. O. Adami, M. Bretthauer, L. Emilsson, M. A. Hernán, M. Kalager, J. F. Ludvigsson, A. Ekbom, The continuing uncertainty about cancer risk in inflammatory bowel disease. *Gut* **65**, 889–893 (2016).
10. S. Olafsson, R. E. McIntyre, T. Coorens, T. Butler, H. Jung, P. S. Robinson, H. Lee-Six, M. A. Sanders, K. Arestang, C. Dawson, M. Tripathi, K. Strongili, Y. Hooks, M. R. Stratton, M. Parkes, I. Martincorena, T. Raine, P. J. Campbell, C. A. Anderson, Somatic evolution in non-neoplastic IBD-affected colon. *Cell* **182**, 672–684.e11 (2020).
11. A. M. Baker, W. Cross, K. Curtius, I. al Bakir, C. H. R. Choi, H. L. Davis, D. Temko, S. Biswas, P. Martinez, M. J. Williams, J. O. Lindsay, R. Feakins, R. Vega, S. J. Hayes, I. P. M. Tomlinson, S. A. C. McDonald, M. Moorghen, A. Silver, J. E. East, N. A. Wright, L. M. Wang, M. Rodriguez-Justo, M. Jansen, A. L. Hart, S. J. Leedham, T. A. Graham, Evolutionary history of human colitis-associated colorectal cancer. *Gut* **68**, 985–995 (2019).
12. J. M. Rhodes, B. J. Campbell, Inflammation and colorectal cancer: IBD-associated and sporadic cancer compared. *Trends Mol. Med.* **8**, 10–16 (2002).
13. J. H. Tsai, P. S. Rabinovitch, D. Huang, T. Small, A. N. Mattis, S. Kakar, W. T. Choi, Association of aneuploidy and flat dysplasia with development of high-grade dysplasia or colorectal cancer in patients with inflammatory bowel disease. *Gastroenterology* **153**, 1492–1495.e4 (2017).
14. M. D. Brugger, T. Valenta, H. Fazilaty, G. Hausmann, K. Basler, Distinct populations of crypt-associated fibroblasts act as signaling hubs to control colon homeostasis. *PLOS Biol.* **18**, e3001032 (2020).
15. C. S. Smillie, M. Biton, J. Ordovas-Montanes, K. M. Sullivan, G. Burgin, D. B. Graham, R. H. Herbst, N. Rogel, M. Slyper, J. Waldman, M. Sud, E. Andrews, G. Velonias, A. L. Haber, K. Jagadeesh, S. Vickovic, J. Yao, C. Stevens, D. Dionne, L. T. Nguyen, A. C. Villani, M. Hofree, E. A. Creasey, H. Huang, O. Rozenblatt-Rosen, J. J. Garber, H. Khalili, A. N. Desch, M. J. Daly, A. N. Ananthakrishnan, A. K. Shalek, R. J. Xavier, A. Regev, Intra- and inter-cellular rewiring of the human colon during ulcerative colitis. *Cell* **178**, 714–730.e22 (2019).
16. L. Kong, V. Pokatayev, A. Lefkovith, G. T. Carter, E. A. Creasey, C. Krishna, S. Subramanian, B. Kochar, O. Ashenberg, H. Lau, A. N. Ananthakrishnan, D. B. Graham, J. Deguine, R. J. Xavier, The landscape of immune dysregulation in Crohn's disease revealed through single-cell transcriptomic profiling in the ileum and colon. *Immunity* **56**, 444–458.e5 (2023).

17. J. C. Martin, C. Chang, G. Boschetti, R. Ungaro, M. Giri, J. A. Grout, K. Gettler, L. S. Chuang, S. Nayar, A. J. Greenstein, M. Dubinsky, L. Walker, A. Leader, J. S. Fine, C. E. Whitehurst, M. L. Mbow, S. Kugathasan, L. A. Denson, J. S. Hyams, J. R. Friedman, P. T. Desai, H. M. Ko, I. Laface, G. Akturk, E. E. Schadt, H. Salmon, S. Gnjatic, A. H. Rahman, M. Merad, J. H. Cho, E. Kenigsberg, Single-cell analysis of Crohn's disease lesions identifies a pathogenic cellular module associated with resistance to anti-TNF therapy. *Cell* **178**, 1493–1508.e20 (2019).
18. G. J. Jasso, A. Jaiswal, M. Varma, T. Laszewski, A. Grauel, A. Omar, N. Silva, G. Dranoff, J. A. Porter, K. Mansfield, V. Cremasco, A. Regev, R. J. Xavier, D. B. Graham, Colon stroma mediates an inflammation-driven fibroblastic response controlling matrix remodeling and healing. *PLOS Biol.* **20**, e3001532 (2022).
19. P. Czarnewski, S. M. Parigi, C. Sorini, O. E. Diaz, S. das, N. Gagliani, E. J. Villablanca, Conserved transcriptomic profile between mouse and human colitis allows unsupervised patient stratification. *Nat. Commun.* **10**, 2892 (2019).
20. S. Kugathasan, L. A. Denson, T. D. Walters, M. O. Kim, U. M. Marigorta, M. Schirmer, K. Mondal, C. Liu, A. Griffiths, J. D. Noe, W. V. Crandall, S. Snapper, S. Rabizadeh, J. R. Rosh, J. M. Shapiro, S. Guthery, D. R. Mack, R. Kellermayer, M. D. Kappelman, S. Steiner, D. E. Moulton, D. Keljo, S. Cohen, M. Oliva-Hemker, M. B. Heyman, A. R. Otley, S. S. Baker, J. S. Evans, B. S. Kirschner, A. S. Patel, D. Ziring, B. C. Trapnell, F. A. Sylvester, M. C. Stephens, R. N. Baldassano, J. F. Markowitz, J. Cho, R. J. Xavier, C. Huttenhower, B. J. Aronow, G. Gibson, J. S. Hyams, M. C. Dubinsky, Prediction of complicated disease course for children newly diagnosed with Crohn's disease: A multicentre inception cohort study. *Lancet* **389**, 1710–1718 (2017).
21. R. F. Leal, N. Planell, R. Kajekar, J. J. Lozano, I. Ordás, I. Dotti, M. Esteller, M. C. Masamunt, H. Parmar, E. Ricart, J. Panés, A. Salas, Identification of inflammatory mediators in patients with Crohn's disease unresponsive to anti-TNFα therapy. *Gut* **64**, 233–242 (2015).
22. T. Nishina, Y. Deguchi, D. Ohshima, W. Takeda, M. Ohtsuka, S. Shichino, S. Ueha, S. Yamazaki, M. Kawauchi, E. Nakamura, C. Nishiyama, Y. Kojima, S. Adachi-Akahane, M. Hasegawa, M. Nakayama, M. Oshima, H. Yagita, K. Shibuya, T. Mikami, N. Inohara, K. Matsushima, N. Tada, H. Nakano, Interleukin-11-expressing fibroblasts have a unique gene signature correlated with poor prognosis of colorectal cancer. *Nat. Commun.* **12**, 2281 (2021).
23. H. Wang, D. H. Wang, X. Yang, Y. Sun, C. S. Yang, Colitis-induced IL11 promotes colon carcinogenesis. *Carcinogenesis* **42**, 557–569 (2021).
24. M. F. Neurath, Cytokines in inflammatory bowel disease. *Nat. Rev. Immunol.* **14**, 329–342 (2014).
25. M. Friedrich, M. Pohin, F. Powrie, Cytokine networks in the pathophysiology of inflammatory bowel disease. *Immunity* **50**, 992–1006 (2019).
26. L. Caradonna, L. Amati, T. Magrone, N. M. Pellegrino, E. Jirillo, D. Caccavo, Enteric bacteria, lipopolysaccharides and related cytokines in inflammatory bowel disease: Biological and clinical significance. *J. Endotoxin Res.* **6**, 205–214 (2000).
27. J. W. Steinke, C. D. Crouse, D. Bradley, K. Hise, K. Lynch, S. E. Kountakis, L. Borish, Characterization of interleukin-4-stimulated nasal polyp fibroblasts. *Am. J. Respir. Cell Mol. Biol.* **30**, 212–219 (2004).
28. E. Sahai, I. Astsaturov, E. Cukierman, D. G. DeNardo, M. Egeblad, R. M. Evans, D. Fearon, F. R. Greten, S. R. Hingorani, T. Hunter, R. O. Hynes, R. K. Jain, T. Janowitz, C. Jorgensen, A. C. Kimmelman, M. G. Kolonin, R. G. Maki, R. S. Powers, E. Puré, D. C. Ramirez, R. Scherz-Shouval, M. H. Sherman, S. Stewart, T. D. Tlsty, D. A. Tuveson, F. M. Watt, V. Weaver, A. T. Weeraratna, Z. Werb, A framework for advancing our understanding of cancer-associated fibroblasts. *Nat. Rev. Cancer* **20**, 174–186 (2020).
29. Y. Hao, S. Hao, E. Andersen-Nissen, W. M. Mauck III, S. Zheng, A. Butler, M. J. Lee, A. J. Wilk, C. Darby, M. Zager, P. Hoffman, M. Stoeckius, E. Papalexi, E. P. Mimitou, J. Jain, A. Srivastava, T. Stuart, L. M. Fleming, B. Yeung, A. J. Rogers, J. M. McElrath, C. A. Blish, R. Gottardo, P. Smibert, R. Satija, Integrated analysis of multimodal single-cell data. *Cell* **184**, 3573–3587.e29 (2021).
30. R. Elmentaite, A. D. B. Ross, K. Roberts, K. R. James, D. Ortmann, T. Gomes, K. Nayak, L. Tuck, S. Pritchard, O. A. Bayraktar, R. Heuschkel, L. Vallier, S. A. Teichmann, M. Zilbauer, Single-cell sequencing of developing human gut reveals transcriptional links to childhood Crohn's disease. *Dev. Cell* **55**, 771–783.e5 (2020).
31. B. Huang, Z. Chen, L. Geng, J. Wang, H. Liang, Y. Cao, H. Chen, W. Huang, M. Su, H. Wang, Y. Xu, Y. Liu, B. Lu, H. Xian, H. Li, H. Li, L. Ren, J. Xie, L. Ye, H. Wang, J. Zhao, P. Chen, L. Zhang, S. Zhao, T. Zhang, B. Xu, D. Che, W. Si, X. Gu, L. Zeng, Y. Wang, D. Li, Y. Zhan, D. Delfouneso, A. M. Lew, J. Cui, W. H. Tang, Y. Zhang, S. Gong, F. Bai, M. Yang, Y. Zhang, Mucosal profiling of pediatric-onset colitis and IBD reveals common pathogenics and therapeutic pathways. *Cell* **179**, 1160–1176.e24 (2019).
32. J. Kinchen, H. H. Chen, K. Parikh, A. Antanaviciute, M. Jagielowicz, D. Fawkner-Corbett, N. Ashley, L. Cubitt, E. Mellado-Gomez, M. Attar, E. Sharma, Q. Wills, R. Bowden, F. C. Richter, D. Ahern, K. D. Puri, J. Henault, F. Gervais, H. Koohy, A. Simmons, Structural remodeling of the human colonic mesenchyme in inflammatory bowel disease. *Cell* **175**, 372–386.e17 (2018).
33. M. D. Brugger, K. Basler, The diverse nature of intestinal fibroblasts in development, homeostasis, and disease. *Trends Cell Biol.* **33**, 834–849 (2023).
34. T. H. Kim, S. J. Choi, Y. H. Lee, G. G. Song, J. D. Ji, Gene expression profile predicting the response to anti-TNF treatment in patients with rheumatoid arthritis; analysis of GEO datasets. *Joint Bone Spine* **81**, 325–330 (2014).
35. J. Z. Liu, S. van Sommeren, H. Huang, S. C. Ng, R. Alberts, A. Takahashi, S. Ripke, J. C. Lee, L. Jostins, T. Shah, S. Abedian, J. H. Cheon, J. Cho, N. E. Daryani, L. Franke, Y. Fuyuno, A. Hart, R. C. Juyal, G. Juyal, W. H. Kim, A. P. Morris, H. Poustchi, W. G. Newman, V. Midha, T. R. Orchard, H. Vahedi, A. Sood, J. J. Y. Sung, R. Malekzadeh, H. J. Westra, K. Yamazaki, S. K. Yang; International Multiple Sclerosis Genetics Consortium; International IBD Genetics Consortium, J. C. Barrett, A. Franke, B. Z. Alizadeh, M. Parkes, T. B K, M. J. Daly, M. Kubo, C. A. Anderson, R. K. Weersma, Association analyses identify 38 susceptibility loci for inflammatory bowel disease and highlight shared genetic risk across populations. *Nat. Genet.* **47**, 979–986 (2015).
36. N. R. West, A. N. Hegazy, B. M. J. Owens, S. J. Bullers, B. Linggi, S. Buonocore, M. Coccia, D. Görtz, S. This, K. Stockenhuber, J. Pott, M. Friedrich, G. Ryzhakov, F. Baribaud, C. Brodmerkel, C. Cieluch, N. Rahman, G. Müller-Newen, R. J. Owens, A. A. Kühl, K. J. Maloy, S. E. Plevy; Oxford IBD Cohort Investigators, S. Keshav, S. P. L. Travis, F. Powrie, Oncostatin M drives intestinal inflammation and predicts response to tumor necrosis factor-neutralizing therapy in patients with inflammatory bowel disease. *Nat. Med.* **23**, 579–589 (2017).
37. T. Sato, D. E. Stange, M. Ferrante, R. G. J. Vries, J. H. van Es, S. van den Brink, W. J. van Houdt, A. Pronk, J. van Gorp, P. D. Siersema, H. Clevers, Long-term expansion of epithelial organoids from human colon, adenoma, adenocarcinoma, and Barrett's epithelium. *Gastroenterology* **141**, 1762–1772 (2011).
38. J. Y. Co, M. Margalef-Català, X. Li, A. T. Mah, C. J. Kuo, D. M. Monack, M. R. Amieva, Controlling epithelial polarity: A human enteroid model for host-pathogen interactions. *Cell Rep.* **26**, 2509–2520.e4 (2019).
39. T. Sato, R. G. Vries, H. J. Snippert, M. van de Wetering, N. Barker, D. E. Stange, J. H. van Es, A. Abo, P. Kujala, P. J. Peters, H. Clevers, Single Lgr5 stem cells build crypt-villus structures in vitro without a mesenchymal niche. *Nature* **459**, 262–265 (2009).
40. G. Lukinavicius, L. Reymond, E. D'Este, A. Masharina, F. Göttfert, H. Ta, A. Güther, M. Fournier, S. Rizzo, H. Waldmann, C. Blaukopf, C. Sommer, D. W. Gerlich, H.-D. Arndt, S. W. Hell, K. Johnsson, Fluorogenic probes for live-cell imaging of the cytoskeleton. *Nat. Methods* **11**, 731–733 (2014).
41. A. N. Anbazhagan, S. Priyamvada, W. A. Alrefai, P. K. Dudeja, Pathophysiology of IBD associated diarrhea. *Tissue Barr.* **6**, e1463897 (2018).
42. T. Duan, O. Cil, J. R. Thiagarajah, A. S. Verkman, Intestinal epithelial potassium channels and CFTR chloride channels activated in ErbB tyrosine kinase inhibitor diarrhea. *JCI Insight* **4**, e126444 (2019).
43. M. Camilleri, J. H. Sellin, K. E. Barrett, Pathophysiology, evaluation, and management of chronic watery diarrhea. *Gastroenterology* **152**, 515–532.e2 (2017).
44. J. R. Thiagarajah, M. Donowitz, A. S. Verkman, Secretory diarrhoea: Mechanisms and emerging therapies. *Nat. Rev. Gastroenterol. Hepatol.* **12**, 446–457 (2015).
45. J. F. Dekkers, C. L. Wiegerinck, H. R. de Jonge, I. Bronsveld, H. M. Janssens, K. M. de Winter-de Groot, A. M. Brandsma, N. W. M. de Jong, M. J. C. Bijvelds, B. J. Scholte, E. E. S. Nieuwenhuis, S. van den Brink, H. Clevers, C. K. van der Ent, S. Middendorp, J. M. Beekman, A functional CFTR assay using primary cystic fibrosis intestinal organoids. *Nat. Med.* **19**, 939–945 (2013).
46. Y. Okada, Ion channels and transporters involved in cell volume regulation and sensor mechanisms. *Cell Biochem. Biophys.* **41**, 233–258 (2004).
47. X. B. Chang, J. A. Tabcharani, Y. X. Hou, T. J. Jensen, N. Kartner, N. Alon, J. W. Hanrahan, J. R. Riordan, Protein kinase A (PKA) still activates CFTR chloride channel after mutagenesis of all 10 PKA consensus phosphorylation sites. *J. Biol. Chem.* **268**, 11304–11311 (1993).
48. P. Sassone-Corsi, The cyclic AMP pathway. *Cold Spring Harb. Perspect. Biol.* **4**, a011148 (2012).
49. E. Ricciotti, G. A. FitzGerald, Prostaglandins and inflammation. *Arterioscler. Thromb. Vasc. Biol.* **31**, 986–1000 (2011).
50. F. A. Fitzpatrick, R. Aguirre, J. E. Pike, F. H. Lincoln, The stability of 13,14-dihydro-15 keto-PGE2. *Prostaglandins* **19**, 917–931 (1980).
51. M. Hamberg, B. Samuelsson, On the metabolism of prostaglandins E 1 and E 2 in man. *J. Biol. Chem.* **246**, 6713–6721 (1971).
52. D. Wang, R. N. DuBois, An inflammatory mediator, prostaglandin E2, in colorectal cancer. *Cancer J.* **19**, 502–510 (2013).
53. J. Jiang, J. Qiu, Q. Li, Z. Shi, Prostaglandin E2 signaling: Alternative target for glioblastoma? *Trends Cancer* **3**, 75–78 (2017).
54. J. W. Regan, EP2 and EP4 prostanoid receptor signaling. *Life Sci.* **74**, 143–153 (2003).
55. P. J. Cook, R. Thomas, P. J. Kingsley, F. Shimizu, D. C. Montrose, L. J. Marnett, V. S. Tabar, A. J. Dannenberg, R. Benezra, Cox-2-derived PGE2 induces Id1-dependent radiation resistance and self-renewal in experimental glioblastoma. *Neuro Oncol.* **18**, 1379–1389 (2016).
56. L. T. Olsen Hult, C. R. Kleiveland, K. Fosnes, M. Jacobsen, T. Lea, EP receptor expression in human intestinal epithelium and localization relative to the stem cell zone of the crypts. *PLOS ONE* **6**, e26816 (2011).
57. A. Horowitz, S. D. Chanez-Paredes, X. Haest, J. R. Turner, Paracellular permeability and tight junction regulation in gut health and disease. *Nat. Rev. Gastroenterol. Hepatol.* **20**, 417–432 (2023).
58. C. L. Dix, H. K. Matthews, M. Uroz, S. McLaren, L. Wolf, N. Heatley, Z. Win, P. Almada, R. Henriques, M. Boutros, X. Trepat, B. Baum, The role of mitotic cell-substrate adhesion re-modeling in animal cell division. *Dev. Cell* **45**, 132–145.e3 (2018).

59. O. M. Lancaster, M. le Berre, A. Dimitracopoulos, D. Bonazzi, E. Zlotek-Zlotkiewicz, R. Picone, T. Duke, M. Piel, B. Baum, Mitotic rounding alters cell geometry to ensure efficient bipolar spindle formation. *Dev. Cell* **25**, 270–283 (2013).
60. A. J. Lomakin, C. J. Cattin, D. Cuvelier, Z. Alraies, M. Molina, G. P. F. Nader, N. Srivastava, P. J. Sáez, J. M. Garcia-Arcos, I. Y. Zhitnyak, A. Bhargava, M. K. Driscoll, E. S. Welf, R. Fiolka, R. J. Petrie, N. S. de Silva, J. M. González-Granado, N. Manel, A. M. Lennon-Duménil, D. J. Müller, M. Piel, The nucleus acts as a ruler tailoring cell responses to spatial constraints. *Science* **370**, eaba2894 (2020).
61. J. Irianto, Y. Xia, C. R. Pfeifer, A. Athirasala, J. Ji, C. Alvey, M. Tewari, R. R. Bennett, S. M. Harding, A. J. Liu, R. A. Greenberg, D. E. Discher, DNA damage follows repair factor depletion and portends genome variation in cancer cells after pore migration. *Curr. Biol.* **27**, 210–223 (2017).
62. Y. Xia, C. R. Pfeifer, K. Zhu, J. Irianto, D. Liu, K. Pannell, E. J. Chen, L. J. Dooling, M. P. Tobin, M. Wang, I. L. Ivanovska, L. R. Smith, R. A. Greenberg, D. E. Discher, Rescue of DNA damage after constricted migration reveals a mechano-regulated threshold for cell cycle. *J. Cell Biol.* **218**, 2545–2563 (2019).
63. R. Li, J. Zhu, Effects of aneuploidy on cell behaviour and function. *Nat. Rev. Mol. Cell Biol.* **23**, 250–265 (2022).
64. W. W. Lim, B. Ng, A. Widjaja, C. Xie, L. Su, N. Ko, S. Y. Lim, X. Y. Kwek, S. Lim, S. A. Cook, S. Schafer, Transgenic interleukin 11 expression causes cross-tissue fibro-inflammation and an inflammatory bowel phenotype in mice. *PLOS ONE* **15**, e0227505 (2020).
65. M. Roulis, R. A. Flavell, Fibroblasts and myofibroblasts of the intestinal lamina propria in physiology and disease. *Differentiation* **92**, 116–131 (2016).
66. J. E. Allen, IL-4 and IL-13: Regulators and effectors of wound repair. *Annu. Rev. Immunol.* **41**, 229–254 (2023).
67. G. Bamias, C. Martin III, M. Mishina, W. G. Ross, J. Rivera-Nieves, M. Marini, F. Cominelli, Proinflammatory effects of TH2 cytokines in a murine model of chronic small intestinal inflammation. *Gastroenterology* **128**, 654–666 (2005).
68. M. T. Kasaian, K. M. Page, S. Fish, A. Brennan, T. A. Cook, K. Moreira, M. Zhang, M. Jesson, K. Marquette, R. Agostinelli, J. Lee, C. M. M. Williams, L. Tchistiakova, P. Thakker, Therapeutic activity of an interleukin-4/interleukin-13 dual antagonist on oxazolone-induced colitis in mice. *Immunology* **143**, 416–427 (2014).
69. S. Fichtner-Feigl, W. Strober, K. Kawakami, R. K. Puri, A. Kitani, IL-13 signaling through the IL-13alpha2 receptor is involved in induction of TGF-beta1 production and fibrosis. *Nat. Med.* **12**, 99–106 (2006).
70. S. Fichtner-Feigl, W. Strober, E. K. Geissler, H. J. Schlitt, Cytokines mediating the induction of chronic colitis and colitis-associated fibrosis. *Mucosal Immunol.* **1**, S24–S27 (2008).
71. A. Wiercinska-Drapalo, R. Flisiak, D. Prokopowicz, Plasma and mucosal prostaglandin E2 as a surrogate marker of ulcerative colitis activity. *Rocz. Akad. Med. Bialymst.* **46**, 60–68 (2001).
72. O. Ahrenstedt, R. Hallgren, L. Knutson, Jejunal release of prostaglandin E2 in Crohn's disease: Relation to disease activity and first-degree relatives. *J. Gastroenterol. Hepatol.* **9**, 539–543 (1994).
73. D. Maseda, A. Banerjee, E. M. Johnson, M. K. Washington, H. Kim, K. S. Lau, L. J. Crofford, mPGES-1-mediated production of PGE(2) and EP4 receptor sensing regulate T cell colonic inflammation. *Front. Immunol.* **9**, 2954 (2018).
74. J. H. An, Prostaglandin E(2) secreted from feline adipose tissue-derived mesenchymal stem cells alleviate DSS-induced colitis by increasing regulatory T cells in mice. *BMC Vet. Res.* **14**, 354 (2018).
75. S. Mukhopadhyay, E. Heinz, I. Porreca, K. Alasoo, A. Yeung, H. T. Yang, T. Schwerd, J. L. Forbester, C. Hale, C. A. Agu, Y. H. Choi, J. Rodrigues, M. Capitani, L. Jostins-Dean, D. C. Thomas, S. Travis, D. Gaffney, W. C. Skarnes, N. Thomson, H. H. Uhlig, G. Dougan, F. Powrie, Loss of IL-10 signaling in macrophages limits bacterial killing driven by prostaglandin E2. *J. Exp. Med.* **217**, e20180649 (2020).
76. Y. Li, C. Soendergaard, F. H. Bergenheim, D. M. Aronoff, G. Milne, L. B. Riis, J. B. Seidelin, K. B. Jensen, O. H. Nielsen, COX-2-PGE(2) signaling impairs intestinal epithelial regeneration and associates with TNF inhibitor responsiveness in ulcerative colitis. *EBioMedicine* **36**, 497–507 (2018).
77. S. Crittenden, M. Goepp, J. Pollock, C. T. Robb, D. J. Smyth, Y. Zhou, R. Andrews, V. Tyrrell, K. Gkikas, A. Adima, R. A. O'Connor, L. Davies, X. F. Li, H. X. Yao, G. T. Ho, X. Zheng, A. Mair, S. Vermeren, B. Z. Qian, D. J. Mole, K. Gerasimidis, J. K. J. Schwarze, R. M. Breyer, M. J. Arends, V. B. O'Donnell, J. P. Iredale, S. M. Anderton, S. Narumiya, R. M. Maizels, A. G. Rossi, S. E. Howie, C. Yao, Prostaglandin E(2) promotes intestinal inflammation via inhibiting microbiota-dependent regulatory T cells. *Sci. Adv.* **7**, eabd7954 (2021).
78. A. Wiercinska-Drapalo, R. Flisiak, D. Prokopowicz, Effects of ulcerative colitis activity on plasma and mucosal prostaglandin E2 concentration. *Prostaglandins Other Lipid Mediat.* **58**, 159–165 (1999).
79. D. S. Rampton, G. E. Sladen, L. J. Youlten, Rectal mucosal prostaglandin E2 release and its relation to disease activity, electrical potential difference, and treatment in ulcerative colitis. *Gut* **21**, 591–596 (1980).
80. M. Roulis, A. Kaklamanos, M. Schernthanner, P. Bielecki, J. Zhao, E. Kaffe, L. S. Frommelt, R. Qu, M. S. Knapp, A. Henriques, N. Chalkidi, V. Koliaraki, J. Jiao, J. R. Brewer, M. Bacher, H. N. Blackburn, X. Zhao, R. M. Breyer, V. Aidinis, D. Jain, B. Su, H. R. Herschman, Y. Kluger, G. Kollias, R. A. Flavell, Paracrine orchestration of intestinal tumorigenesis by a mesenchymal niche. *Nature* **580**, 524–529 (2020).
81. A. E. F. Sheppe, E. Kummari, A. Walker, A. Richards, W. W. Hui, J. H. Lee, L. Mangum, A. Borazjani, M. K. Ross, M. J. Edelmann, PGE2 augments inflammasome activation and M1 polarization in macrophages infected with *Salmonella typhimurium* and *Yersinia enterocolitica*. *Front. Microbiol.* **9**, 2447 (2018).
82. P. D. Bozyk, B. B. Moore, Prostaglandin E2 and the pathogenesis of pulmonary fibrosis. *Am. J. Respir. Cell Mol. Biol.* **45**, 445–452 (2011).
83. J. M. McCoy, J. R. Wicks, L. P. Audoly, The role of prostaglandin E2 receptors in the pathogenesis of rheumatoid arthritis. *J. Clin. Invest.* **110**, 651–658 (2002).
84. R. Nasrallah, R. Hassouneh, R. L. Hebert, Chronic kidney disease: Targeting prostaglandin E2 receptors. *Am. J. Physiol. Renal Physiol.* **307**, F243–F250 (2014).
85. T. G. Lauridsen, H. Vase, J. Starklint, C. C. Graffe, J. N. Bech, S. Nielsen, E. B. Pedersen, Increased renal sodium absorption by inhibition of prostaglandin synthesis during fasting in healthy man. A possible role of the epithelial sodium channels. *BMC Nephrol.* **11**, 28 (2010).
86. L. Jostins, Host-microbe interactions have shaped the genetic architecture of inflammatory bowel disease. *Nature* **491**, 119–124 (2012).
87. J. V. Patankar, T. M. Müller, S. Kantham, M. G. Acera, F. Mascia, K. Scheibe, M. Mahapatro, C. Heichler, Y. Yu, W. Li, B. Ruder, C. Günther, M. Leppkes, M. J. Mathew, S. Wirtz, C. Neufert, A. A. Kühl, J. Paquette, K. Jacobson, R. Atreya, S. Zundler, M. F. Neurath, R. N. Young, C. Becker, E-type prostanoid receptor 4 drives resolution of intestinal inflammation by blocking epithelial necroptosis. *Nat. Cell Biol.* **23**, 796–807 (2021).
88. J. W. Squair, M. Gautier, C. Kathe, M. A. Anderson, N. D. James, T. H. Hutson, R. Hudelle, T. Qaiser, K. J. E. Matson, Q. Barraud, A. J. Levine, G. la Manno, M. A. Skinnider, G. Courtine, Confronting false discoveries in single-cell differential expression. *Nat. Commun.* **12**, 5692 (2021).


**Acknowledgments:** We thank L. D. Orzolek and T. J. Creamer from the Johns Hopkins Single Cell and Transcriptomics Core for conducting single-cell RNA-sequencing. We thank H. Zhang from Johns Hopkins Bloomberg Flow Cytometry and Immunology Core for performing cell sorting. We thank L. Roker and H. West-Foyle from the Johns Hopkins Microscope Facility for suggestions with electron and confocal microscopy. We thank B. Bleck from Takeda Pharmaceuticals for insightful discussions. We thank H. Wang from the Mechanical Biology Institute of the National University of Singapore for insightful discussions. We thank S. Ramachandran and J. McNamara from the Johns Hopkins Department of Cell Biology for insightful discussions. **Funding:** This work was supported by Takeda Development Center Americas Inc. #137883. B.A.J. and A.Z.L. received support from the NIH Medical Scientist Training Program T32GM136577. **Author contributions:** Conceptualization: Y.D. and R.L. Methodology: Y.D., T.C.L., and M.D. Investigation: Y.D., B.A.J., L.R., M.Z., T.B., A.Z.L., S.R., I.C., J.Z., B.S., and N.Z. Resources: T.C.L., S.W., and P.S. Manuscript writing: Y.D., T.C.L., and R.L. Manuscript review and editing: Y.D., J.Z., T.C.L., M.D., and R.L. Visualization: Y.D. Supervision: T.C.L. and R.L. Funding acquisition: T.C.L. and R.L. **Competing interests:** The authors declare that they have no competing interests. **Data and materials availability:** The scRNA-seq data are deposited to the NCBI GEO repository (GSE237034). All data needed to evaluate the conclusions in the paper are present in the paper and/or the Supplementary Materials.

Submitted 15 July 2023
Accepted 27 February 2024
Published 3 April 2024
10.1126/sciadv.adj7666